NSP

Monticello Nuclear Power Plant

Qualification of Reactor Physics Methods for Application to Monticello

NSPNAD-8609, Rev 2

August 1994

Northern States Power Company
Nuclear Analysis & Design

MTB
8/25/94

NSP

Monticello Nuclear Power Plant

Qualification of Reactor Physics Methods for Application to Monticello

NSPNAD-8609, Rev 2

August 1994

Northern States Power Company
Nuclear Analysis & Design

[redacted]

MTO
8/25/94

MONTICELLO NUCLEAR GENERATING PLANT

QUALIFICATION OF REACTOR PHYSICS METHODS

FOR

APPLICATION TO MONTICELLO

NSPNAD-8609

Revision 2

August 1994

Principal Contributors

Anthony Bockelman, NSP
Clifford Bonneau, NSP
David Dean, NSP
Keith Dehnbostel, NSP
Thomas Iseman, NSP
William Lax, NSP
Ryan Maas, NSP
Michael Miller, NSP
Peter Pankratz, NSP
Richard Rohrer, NSP
Ralph Rye, NSP
Richard Streng, NSP
Scott Vanevenhoven, NSP

Prepared by _____ Date 8/23/94
David W. Dean, Principal Engineer

Reviewed by _____ Date 8/23/94
Clifford A. Bonneau, Process Manager

Approved by _____ Date 8/24/94
Louis P. Matis, Director Fuel Resources

ABSTRACT

This document is a Topical Report describing the Northern States Power Company (NSP) qualification of reactor physics methods for application to the Monticello Nuclear Plant.

This document addresses the reactor model description, qualification and quantification of reliability factors and applications to operations and reload safety evaluations of the Monticello plant.

LEGAL NOTICE

TABLE OF CONTENTS

LIST OF TABLES

LIST OF FIGURES

1.0 INTRODUCTION

This report addresses the reactor model description, qualification and quantification of reliability factors, applications to operations and reload safety evaluations of the Monticello Nuclear Plant (Mnt). This model, based on the Studsvik CMS system of codes, can be used as a substitute for the CASMO/NDH methods previously approved for use (Reference 2). Adoption of the methods described here does not preclude the use the earlier CASMO/NDH methods as needed.

A summary description of the computer codes is given in Section 2. This report stresses the aspects of implementation of the NSP model; the individual code descriptions are referenced in Appendix B.

Whenever possible, directly observable parameters (such as reactor critical k_{eff} and measured incore detector fission rates) are utilized. The Mnt data used in this evaluation span cycles 11 through 15. In order to be completely objective in the choice of data to be used for the comparisons, all Mnt cycles 11 through 15 measurements were reviewed and qualified prior to initiating the comparison calculations.

After the measured data to be used in the benchmark process had been defined, the model calculations were performed and comparisons are presented in this report as part of the quantification of the NSP model calculational uncertainties and reliability factors. A statistical approach was used to derive the uncertainties. These uncertainties are consistent with the model application procedures and methodology.

The uncertainties are evaluated by direct comparison to experimental data.

In order to provide a continuing verification of the conservatism of the reliability factors determined by Mnt cycles 11 through 15 data, ongoing comparisons are made each cycle using the statistical methods described in this report. A discussion of the reliability factors is provided in Section 3.

The methods for use of the model and the reliability factors are described relative to reactor operation and reload safety evaluation in Sections 4 and 5.

2.0 GENERAL CHARACTERISTICS OF THE NSP CALCULATIONAL MODEL

The Monticello (Mnt) calculational model based on the Studsvik system of codes, is very similar to the calculational model previously approved for use by Yankee Atomic Electric Company for use with Vermont Yankee (see References 4, 5, and 6), and is similar in many respects to the model previously approved for use with Mnt (see Reference 2). A flow diagram of the Monticello model is shown in Figure 2.0.1. The code acronyms used in these figures are defined in Appendix B.

In general, the CASMO-3[7,8] program is used to generate the lattice physics parameters for input to SIMULATE-3[11,12]. MICBURN-3[10] is used to model gadolinia containing fuel pins and provides homogenized Gd cross sections for input to CASMO-3. CASMO-3 produces fission product nuclide concentrations, depletion and product chain data, pin power distributions, microscopic and macroscopic cross sections, and other nuclear data input to TABLES-3[13]. TABLES-3 constructs tables of these nuclear data as functions of local state variables (e.g. water density, fuel temperature etc.) for input to SIMULATE-3.

SIMULATE-3 is a three-dimensional, two-group steady state reactor neutronic and thermal hydraulic simulator. This simulator is used to generate eigenvalues, power distributions, and incore instrument predictions for use in reload safety evaluations, plant support, reload

design, fuel management, and benchmark comparisons.

ESCORE[15,16,17,18] is an EPRI computer code for steady state fuel performance analysis. The Monticello methodology uses ESCORE for fuel temperature predictions to be used as input to MICBURN-3, CASMO-3, and SIMULATE-3 for modeling fuel temperature related effects on the nuclear data (i.e. Doppler coefficient and power defect).

The S3POST[14] program summarizes SIMULATE-3 results including the measured and predicted incore reaction rates. SPM, an NSP developed code, then combines all the statepoints to calculate overall uncertainties.

The computer code descriptions are summarized in Appendix B.

Figure 2.0.1 Flow Chart: CASMO-3/SIMULATE-3 Model

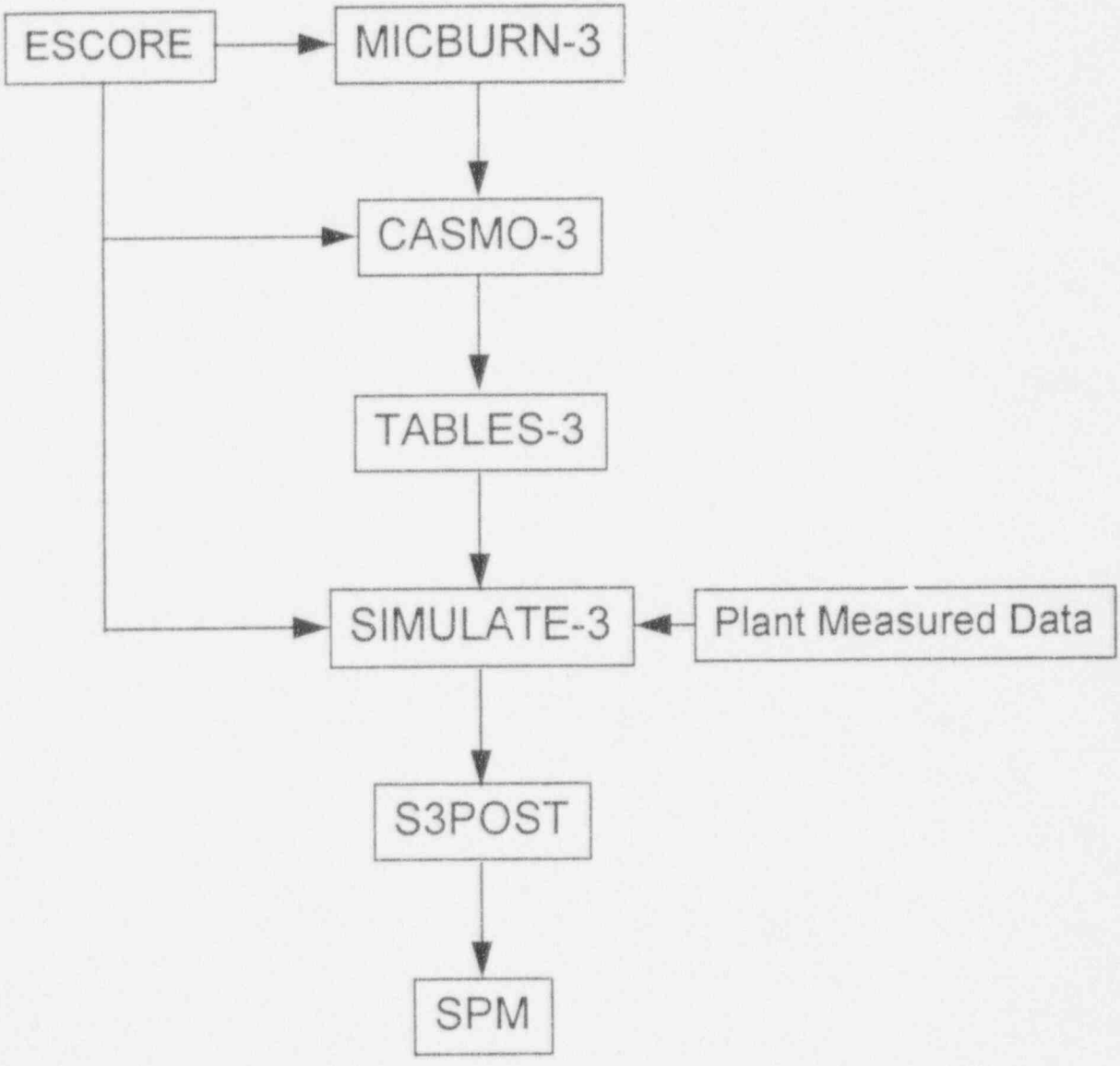

3.0 MODEL VERIFICATION AND RELIABILITY FACTOR DETERMINATION

The NSP models have been benchmarked against Mnt measurements made during cycles 11 through 15 for the CASMO-3/SIMULATE-3 model to quantify the reliability factors to be used in safety related calculations. The resultant reliability factors and biases are summarized in Table 3.0.1. The remainder of this section is a detailed account of the derivation of these factors.

The term reliability factor (RF) is used to describe the allowances to be used in safety related calculations to assure conservatism. The uncertainty factor (1σ) is used to describe the actual model accuracy. The reliability factor is always larger than the uncertainty factor.

The term bias is used to describe the statistical difference between an observed or measured distribution and the calculated value.

Appendix A describes the statistical methods used in the evaluation of the uncertainties in the following sections.

During each cycle, measured and calculated parameters will be compared in order to verify and update the reliability factors determined in this section. Results of the verification and an update for each parameter will be documented in the reload safety evaluation for the reload in which the updated values will be used. The updates to the reliability factors will be in accordance with the methods outlined in this section and in Appendix A.

TABLE 3.0.1 Reliability Factors for Monticello

Parameter	Reliability Factor (expressed as applied)	Reliability Factor (expressed as %)	Bias
APLHGR	RF_{TPF} = .124	12.4	0
LHGR	RF_{TPF} = .124	12.4	0
MCPR	RF_{RPF} = .095	9.5	0
Rod Worth	RF_{RODS} = .10	10.0	0
Void Coefficient	RF_{VOIDS} = .10	10.0	0
Doppler Coefficient	RF_{DOP} = .10	10.0	0
Delayed Neutron Parameters			
Λ	RF_{Λ} = .04	4.0	0
β	RF_{β} = .04	4.0	0

3.1 Control Rod Worth

Control rod worth in a BWR cannot be directly measured. Control rod worth can be inferred from various reactor critical conditions. The approach taken is to benchmark the NSP model to these critical conditions. The data base includes 9 few rod criticals and 24 sequence criticals taken at temperatures ranging from 85 °F to 209 °F. This data represents the actual critical statepoints in cycles 11 through 15. All measured statepoints at temperatures below the boiling point of 212 °F have been included. The results of the comparisons are shown in Table 3.1.1.

The standard deviation of the calculated k_{eff} at the critical positions is .0027. This difference includes the measurement uncertainty as well as the calculational uncertainty. The typical amount of reactivity being held down by rods is on the order of 10% Δk. Using this value we can calculate an uncertainty in rod worth by dividing the standard deviation by this worth, i.e. .27% Δk / 10% Δk = 2.7%. For conservatism the rod worth reliability factor (RF_{rods}) is defined as 10%.

Figures 3.1.1 through 3.1.5 present graphs of control rod notch inventory versus cycle exposure for hot critical conditions for cycles 11 through 15. The best estimate is the predicted control rod notch inventory using CASMO-3/SIMULATE-3 with the $\pm 1\% \Delta K$ reactivity anomaly shown. Measured rod notch inventory is indicated as a dot for each statepoint. All measured values are within the $\pm 1\% \Delta K$ bounds. This indicates the well behaved prediction of the model and supports the use of the conservative rod worth reliability factor used above.

Table 3.1.1 Measured to Calculated Rod Worth Comparison

Cycle	Notches Withdrawn	Core Ave. Exposure (GWD/MTU)	Temperature (°F)	k_{eff}
11	60	12.802	85	0.9921
	64	12.802	106	0.9936
	644	12.802	106	0.9948
	394	12.802	113	0.9936
12	152	13.666	129	0.9964
	1416	13.666	128	0.9928
	728	13.666	128	0.9938
	734	16.922	141	0.9903
	1498	19.926	206	0.9896
13	66	15.025	91	0.9905
	106	15.025	91	0.9904
	978	15.025	91	0.9897
	678	15.025	91	0.9908
	2040	23.878	200	0.9876
	1518	24.789	164	0.9851
14	118	16.683	109	0.9907
	1076	16.683	111	0.9913
	734	16.683	118	0.9936
	108	21.252	122	0.9924
	864	21.252	123	0.9919
	738	22.494	152	0.9895
	892	23.330	209	0.9905
	1502	25.193	154	0.9923
	1542	25.193	142	0.9920
15	118	16.217	108	0.9933
	114	16.217	108	0.9963
	984	16.217	113	0.9939
	774	16.217	107	0.9963
	2560	16.310	200	0.9979
	1516	16.310	147	0.9962
	1632	17.833	181	0.9939
	762	20.368	137	0.9922
	702	22.419	129	0.9928

Mean k_{eff} = 0.9923 σ = .0027

Figure 3.1.1
Control Notch Worth Inventory Versus Exposure
Cycle 11

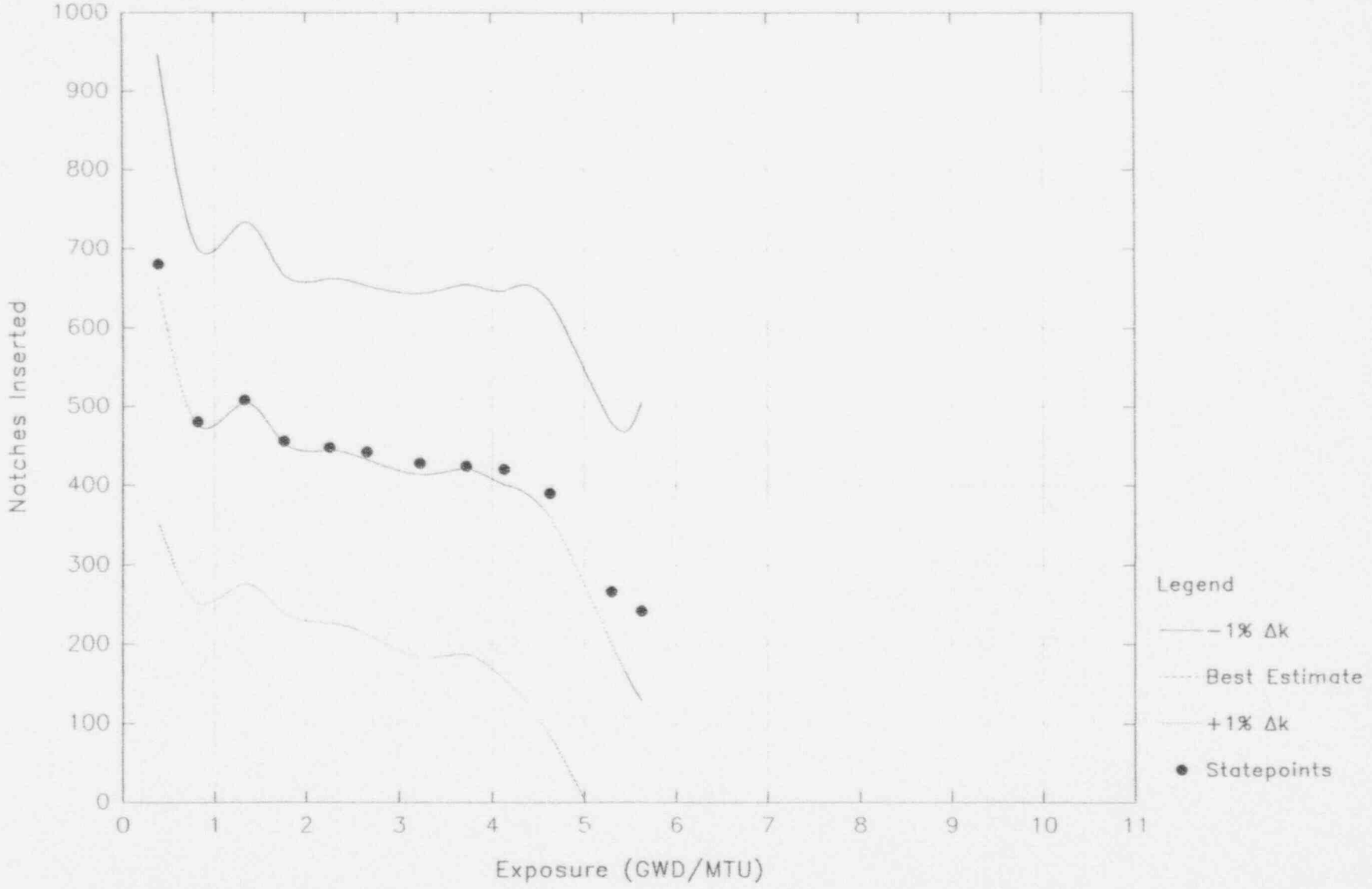

Figure 3.1.2
Control Notch Worth Inventory Versus Exposure
Cycle 12

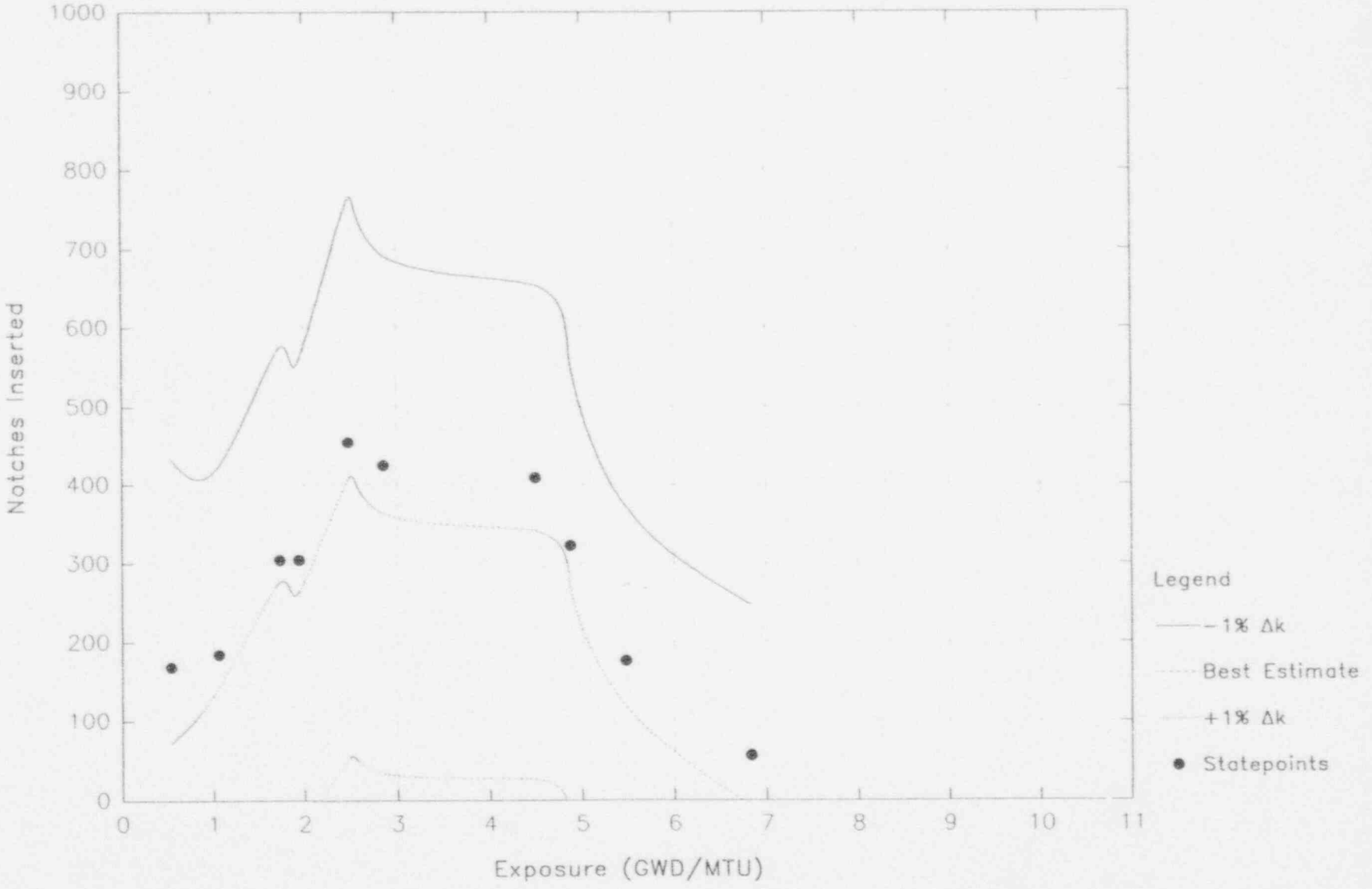

Figure 3.1.3
Control Notch Worth Inventory Versus Exposure
Cycle 13

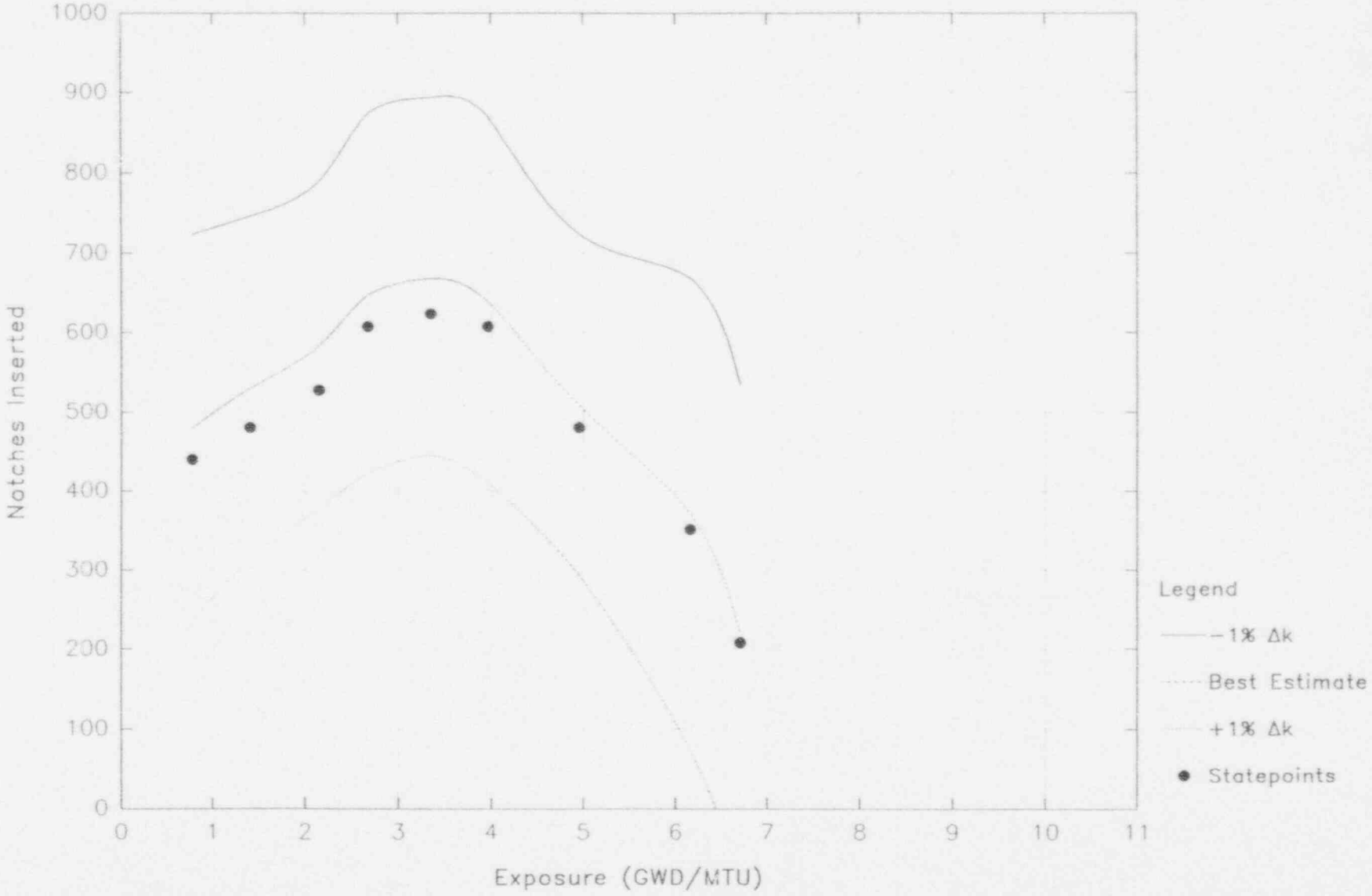

Figure 3.1.4
Control Notch Worth Inventory Versus Exposure
Cycle 14

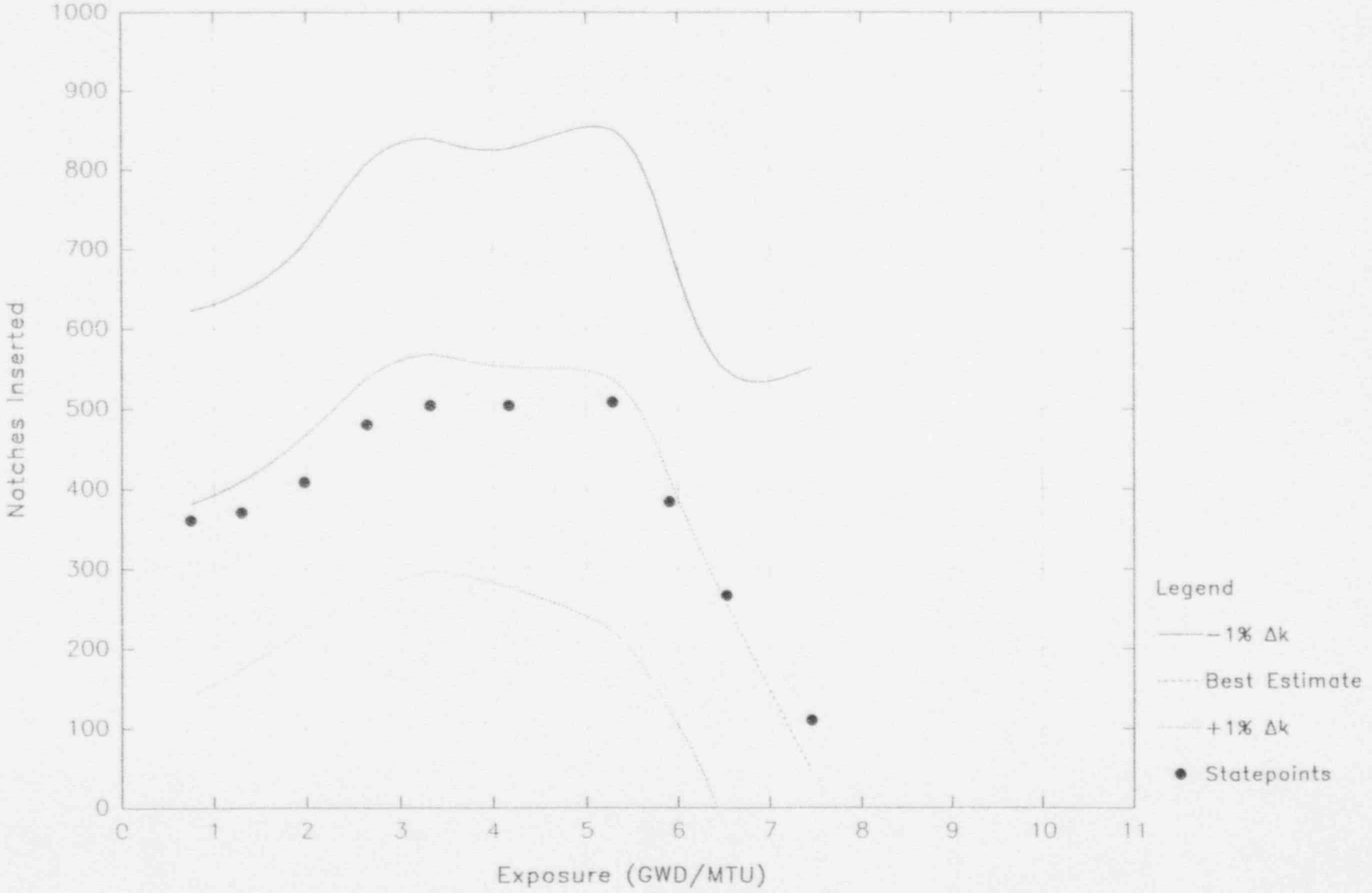

Figure 3.1.5
Control Notch Worth Inventory Versus Exposure
Cycle 15

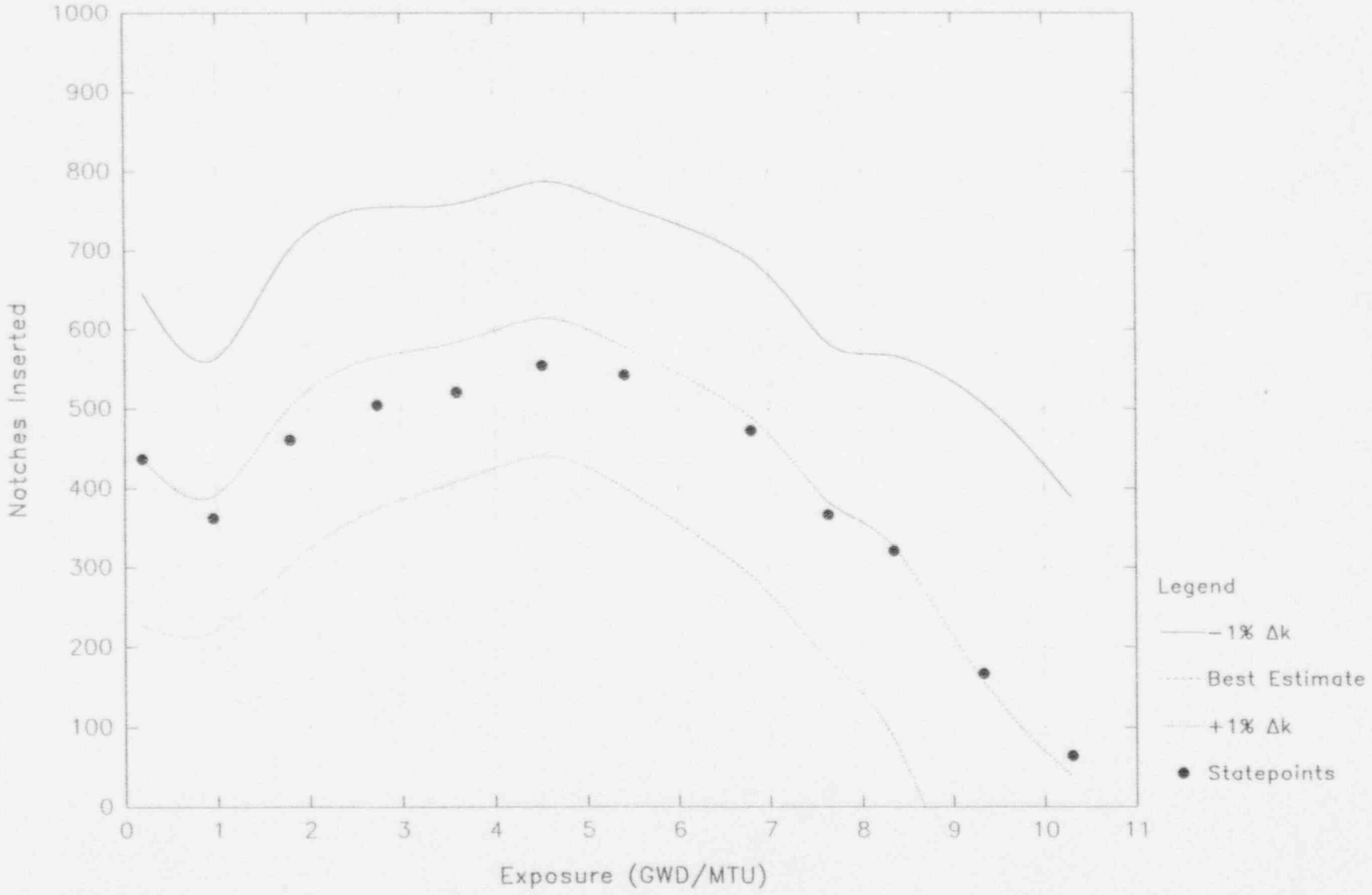

3.2 Temperature Coefficient

The range of values of moderator temperature coefficients encountered in current BWR lattices does not include any that are significant from the safety point of view. The small magnitude of this coefficient, relative to that associated with steam voids and combined with the long time-constant associated with transfer of heat from the fuel to the coolant, makes the reactivity contribution of moderator temperature change insignificant during rapid transients.

For the reasons stated above, current core design criteria do not impose limits on the value of the temperature coefficient, and effects of minor design changes on the coefficient usually are not calculated.

3.3 Void Coefficient

The void coefficient in a BWR cannot be directly measured, i.e., there are always present the effects of other parameters such as control rods, Doppler coefficient, xenon etc. The magnitude of the uncertainty in the void coefficient can be inferred, however, from comparisons of predicted versus measured critical statepoints where the effect of the other parameters is minimized. Table 3.3.1 gives calculated values for the measured critical statepoints from EOC coastdown for cycles 11 through 15. The standard deviation of the calculated k_{eff}'s is ± .0020 Δk for the coastdown cases. The total core reactivity held down by voids for the average void fraction (35%) at full power is on the order of 5% Δk. An average $\%\Delta k/\%\Delta V$ can be calculated from Table 3.3.1 which represents the error in the predicted and measured value. $\% \Delta k/\% \Delta V = .0083$. Multiplying by the average percent void gives the error in terms of Δk. $\% \Delta k = .0083 * 35\% = 0.29\%$. Therefore the uncertainty in void can be calculated by dividing by the total void worth at 35% which gives 0.29% / 5% = 5.8% uncertainty. This uncertainty includes components of error from exposure, xenon and Doppler. Therefore, a reliability factor of 10% in void coefficient is deemed appropriately conservative for safety related calculation.

Table 3.3.1 EOC Coastdown Statepoints

Cycle	Cycle Exposure (GWD/MTU)	Power (%)	Void (%)	k_{eff}
11	5.624	100	34.5	1.0009
	6.352	99	36.9	1.0017
	6.756	92	34.3	1.0016
	7.256	84	31.0	1.0015
	7.764	74	27.6	1.0014
	8.159	66	24.7	1.0016
12	5.478	100	37.8	1.0002
	6.830	96	33.2	1.0004
	7.148	91	32.7	0.9999
13	7.373	100	36.7	0.9975
	8.229	87	31.4	0.9970
	8.724	78	28.3	0.9968
	9.103	71	25.7	0.9969
	9.729	59	21.4	0.9969
	10.165	51	18.4	0.9968
14	7.454	100	35.8	0.9992
	8.237	93	33.7	0.9990
	8.882	83	29.8	0.9988
15	9.332	100	32.1	0.9982
	10.301	91	29.8	0.9972
	11.197	73	25.0	0.9960

Mean K_{eff} = .9990 σ =.0020

3.4 Doppler Coefficient

Measurements can be made in a power reactor which are directed at determining the Doppler coefficient at various power levels. In a BWR the uncertainty associated with such measurements (e.g. rod repositioning, void feedback) are such that results are not reliable for direct validation of the calculational model. Consequently, an indirect approach is taken.

The primary variable in the calculation of Doppler effects using the CASMO-3/SIMULATE-3 model is the fuel temperature. A change in fuel temperature associated with a power change results in a reactivity change due to the change in the resonance absorption.

The algorithm in SIMULATE-3 that determines the model change in reactivity due to the fuel temperature change uses data calculated by CASMO-3. The approach is to determine the accuracy of CASMO-3 in calculating the change in the resonance integral (RI) due to a known fuel temperature increase, then use engineering judgement to bound this uncertainty to assure conservatism.

Comparisons of CASMO-3 calculations to critical experiments (references 4, 23, 24, 25, 26, 27, 28, and 33) have determined that the uncertainty of CASMO-3 is well within the measurement uncertainty. In view of this, a 10% reliability factor placed on the Doppler coefficient is judged adequate to assure a conservative value.

3.5 Isotopics

The benchmarking of CASMO-3 to Yankee Rowe and Zion data is thoroughly discussed in references 4 and 36.

3.6 Power Distribution Reliability Factor Determination

The purpose of this section is to discuss the methods used to determine the power distribution reliability factors. Reliability factors have been determined for the local fuel pin power in a node and for the total fuel bundle power. These factors can then be applied to the calculation of the linear heat generation rate (LHGR), the average planar linear heat generation rate (APLHGR) and the critical power ratio (CPR) respectively.

The statistics presented in Sections 3.6.1 and 3.6.2 follow those presented in the Prairie Island Topical, see reference 1.

3.6.1 Local Power Distribution

The model reliability factor for calculating power distributions is based on comparisons of measured and predicted traversing incore probe (TIP) flux detector signals for normal operating core conditions.

The signals from the detectors are corrected by the on-site process computer to account for such things as detector sensitivity, drift, and background. It is these corrected signals, or reaction rates, which have been compared to simulated reaction rates calculated with the NSP models in order to derive model reliability factors.

The reliability factor, RF, is defined as a single value of $\Delta TPF/TPF_m$ such that TPF_c (I,J,K) times 1 + $\Delta TPF/TPF_m$ has a 95% probability at a 95% confidence level of being conservative with respect to TPF_m (I,J,K). The subscripts c and m denote calculated and measured values. TPF (I,J,K) is the total pin peaking factor for all I,J,K locations in the core. This value cannot be measured directly. What is measured by the detector system is the

reaction rate in the instrument thimble. This measured reaction rate is a local value. $RR_m = \phi\Sigma_f$ (measured).

These measurements are collapsed down to 24 axial nodal values in each thimble consistent with the nodalization of SIMULATE-3. The CASMO-3/SIMULATE-3 model has been used to calculate the reaction rates in the instrument thimbles: $RR_c = \phi\Sigma_f$(calculated). The observed difference distribution (ODD) has then been calculated by simply taking the relative difference of these two values:

$$ODD = (RR_m - RR_c) / RR_m$$

for all measured locations in the core.

It is important to note that the ODD is <u>not</u> the difference between nodal powers but rather is the difference between <u>local</u> fission rate values. It is assumed that the ODD is equal to $\Delta TPF/TPF_m$. This is a valid assumption since the calculated and measured reaction rates are local fission rate values as is the TPF, the only difference is the location.

The observed difference distribution determined above includes the uncertainties in the calculational model as well as the uncertainties in the measurement instrumentation. The calculational model uncertainty includes uncertainty in the calculation of the nodal power and in the conversion factors from nodal power to the pin power which is taken to be the same as the total uncertainty in the calculated reaction rates. Therefore, the total uncertainty in the local pin power can be written as follows:

$$RF_{TPF} = \sigma_{TPF,95}$$

where $\sigma_{TPF,95}$ is determined from the ODD determined above.

The simulated detector signals are calculated in a manner which is consistent with the calculation of local power peaking factors for the purpose of safety evaluations; see Section 5.1. The first step is to compute the power distribution under consideration. The resolution used is 24 axial levels per fuel assembly.

The predicted detector signals are obtained directly from SIMULATE-3 calculated two group fluxes and fission cross sections in the instrument locations.

A total of 68 core statepoints, or TIP traces, were chosen for the purpose of comparing measured and simulated in-core reaction rates for the CASMO-3/SIMULATE-3 model. These statepoints span operating cycles 11 through 15 of Monticello. The specific core conditions for each of the statepoints are given in Table 3.6.1.

Typical examples of the comparisons of measured and predicted reaction rates are provided in Figures 3.6.1 through 3.6.15. The data is presented in sets of three figures, one set for each cycle, three TIP trace maps per cycle (BOC, MOC, EOC). Each figure in each set presents the differences between the measured and predicted axial reaction rates for all instrumented locations in the core and the core average axial reaction rates (lower right hand corner).

The measurements are represented as squares at the 24 axial levels. The predicted reaction rates are shown as lines.

The distribution of observed differences between measured and calculated instrument signals for all 68 core statepoints was determined. For each trace, 2 of the 24 axial values were excluded

from consideration. These excluded values correspond to the top and bottom nodes. These locations are areas of steep flux gradients, and small errors in instrument position result in large differences in measured to calculated values. Since the reaction rates in these areas are always smaller (i.e., the high power point will never occur in the top or bottom nodes) these values were excluded from the determination of the observed differences density function. The reliability factors developed here include the measurement uncertainty as well as the calculational uncertainty. However, known problems with the TIP measurement system such as TIP tube mislocation and channel bowing make the measurement uncertainty very large relative to the calculational uncertainty. A 95%/95% confidence level was determined from the observed difference density function determined above.

The method of normalizing the calculated and measured reaction rates was used to adjust the average of all 24 detectors at the remaining 22 axial locations to 1.0. This normalization technique was used to put the measured and predicted values on a common basis which is consistent with the definition of the local peaking factors. The measurement uncertainty in core thermal power is accounted for in the transient and LOCA analysis.

All data was retained in the data base. The total number of nodal observations used was 35,904. The total number of observations eliminated was 3,264.

All subsequent statistical analysis has been performed using the methods described in Appendix A.2. To ensure a conservative reliability factor at all power levels, the sample was divided into subsamples as a function of power (see Figure 3.6.22). A standard deviation was calculated for each subsample using the methods described in Appendix A.2. Figure 3.6.22 shows a distinct power dependence for the absolute difference. Therefore, to assure conservatism in the application, the reliability factor will be applied as a relative rather than an absolute value.

The distribution of observed differences is shown in Figure 3.6.16. The following statistics therefore represent the total data base as described above using relative differences.
The first step using this method is to determine the mean relative difference of the measured to calculated values (μmc) and the standard deviation (σmc):

$$\mu mc = \frac{\sum_{i=1}^{n} e_i}{n} = 0.002$$

$$\sigma mc = \sqrt{\frac{\sum_{i=1}^{n} (e_i - \mu mc)^2}{n-1}} = 0.071$$

where: e_i = ith observed difference
n = total number of observations

The second step is to transform the e_i to standard measure using

the following formula:

$$Z_i = \frac{e_i - \mu mc}{\sigma mc}$$

and the resulting variates Z were then sorted into ascending order(see Figure 3.6.17). A value of Z was chosen as an estimate of the 95th percentile of the distribution, i = 34,109. This gives the 95th percentile of Z to be

$$Z_{34109} = Q_{95} = 1.689$$

which implies that 95% of the errors are likely to be less than 1.689 standard deviations from the mean. It remains then to calculate a 95% confidence interval on Q_{95} using the following formula

$$Var Q_{95} = \sigma^2_{Q95} = \frac{q(1-q)}{n\, f_i^2}$$

where:
- q = the quantile (.95)
- n = number of independent observations in sample
- f_i = ordinate of the density function of the distribution function at the abscissa q

Due to the dependence of the observed differences with axial height, the total number of observations was reduced by a factor of 5 to determine the total number of independent observations. The factor of 5 was chosen to conservative bound based on the Prairie Island topical, Reference 1, value of 3.0 which is applicable to 48 axial data points rather than 24.

It is necessary to obtain an estimate of $f_i(.95)$, and this was done by applying a linear regression analysis on a short interval of the cumulative distribution function (CDF) of Z in the region of the 95th percentile (see Figure 3.6.18). The estimated slope of the CDF (estimated from the straight line in Figure 3.6.18) is an estimate of the ordinate density function. The slope is calculated as 0.143.

This gives:

$$Var Q_{95} = \frac{0.95(1-0.95)}{\left[\frac{35904}{5}\right] 0.143^2} = 0.00032$$

and

$$\sigma_{Q95} = \sqrt{Var Q_{95}} = 0.018$$

The estimate of the upper limit on Q_{95} is

$$K_c\, \sigma_{Q95} = 1.645 \cdot 0.018 = 0.029$$

thus:

$$Q_{95} \leq 1.689+0.029$$

The upper limit is then 1.689 + .029 = 1.718 which gives the following as the 95% confidence level that the calculated reaction rate (RR_c) will be conservative with respect to the measured reaction rate (RR_m).

$$RR_m = RR_c\ (1 + \mu mc + (Q_{95} + K_C\sigma_{Q95})\sigma mc)$$
$$RR_m = RR_c\ (1 + .124)$$

Therefore $\sigma_{TPF,95}$ = .124 with the bias absorbed into the reliability factor. Note that this value includes measurement error which adds conservatism to the calculation.

3.6.2 Integrated Power Distribution

The model reliability factors for calculating power distributions are based on comparisons of integrated measured and predicted TIP trace signals obtained from normal operating core conditions.

The reliability factor (RF) is defined as a single value of $\Delta RPF/RPF_m$ such that RPF(I,J) calculated times 1 + $\Delta RPF/RPF_m$ has a 95% probability at a 95% confidence level of being conservative with respect to the measured RPF(I,J). The subscripts c and m will be used to denote calculated and measured values. RPF(I,J) is the integrated peaking factor determined for all I,J locations in the core. This value cannot be measured directly. What is measured by the detector system is the reaction rate in the instrument thimble. This measured reaction rate is a local value. $IRR_m = \phi\Sigma_f$ (measured). These values are determined at each thimble by integrating the central 22 measured axial locations. The three-dimensional model CASMO-3/SIMULATE-3 has been used to calculate the reaction rate in the instrument thimbles. $IRR_c = \phi\Sigma_f$ (calculated).

The observed difference distribution (ODD) has then been calculated by simply taking the relative difference of these two values

ODD = $(IRR_m - IRR_c)/IRR_m$ for all measured locations in the core.

The observed difference distribution determined above includes the uncertainties in the calculational model, the uncertainties in the measurement instrumentation, and the uncertainties in conversion factors from nodal power to instrument value. The calculational model uncertainty includes uncertainty in the calculation of the nodal powers as well as uncertainties in the local pin powers. Therefore the uncertainty in the local integrated pin power can be written as follows:

$$RF_{\Delta RPF} = \sigma_{RPF,95}$$

where $\sigma_{RPF,95}$ is determined from the ODD.

The distribution of observed differences between measured and calculated integrated instrument signals for all 68 statepoints was determined for the CASMO-3/SIMULATE-3 model and is shown in Figure 3.6.19. The total number of integrated observations used was 1,632.

All subsequent statistical analysis has been performed using the methods described in Appendix A.2 on the entire sample.

The cumulative distribution function and the CDF in the region of the 95th percentile are given in Figures 3.6.20 and 3.6.21 respectively. The significant parameters calculated for this distribution are as follows:

μmc = 0.001
σmc = 0.043
Q_{95} = 1.728
σ_{Q95} = 0.035
$K_c \sigma_{Q95}$ = 0.058
$IRR_{.95}$ = IRR_c (1 + 0.079)
$\sigma_{RPF.95}$ = 0.079

where: IRR_m = Integrated reaction rate measured
IRR_c = Integrated reaction rate calculated

For conservatism the reliability factor will remain at the value determined for CASMO-2/NDH (reference 2) as

$$RF_{RPF} = 0.095 > \sigma_{RPF.95} = 0.079$$

No dependence of the observed difference with position was found. Therefore, n was not reduced.

3.6.3 Gamma Scan Comparisons

Gamma scan measurements are not available from Mnt cycles 11 through 15. The reliability factors for the CASMO-2/NDH methods (Reference 2) were determined from TIP comparisons which bounded the gamma scan comparisons. The greater measurement uncertainties associated with neutron TIPs results in larger measured to calculated variance as compared to gamma scan. Therefore, use of neutron TIP statistics, including the measurement uncertainty, will result in a conservative estimate of the power distribution uncertainty.

Other benchmarks of the CASMO-3/SIMULATE-3 power distribution predictions are available for gamma scan (references 4, and 35), critical experiments (references 4, 28, 32, 33, 34, 38, and 51), fine mesh PDQ (diffusion theory) (references 5, 37, 41, 42, 44, and 46), CASMO-3 color sets (references 5, 34, 41, 46, and 48), gamma TIPs (references 5, 6, 40, and 45), and neutron TIPs (references 5, 37, 38, 39, 41, 45, 47, 49, and 50). These comparisons include both BWR and PWR type cores and geometries.

3.6.4 Standard Power Distribution Comparison

The following is a presentation of the power distribution using the industry standard format. Published power distribution data is usually presented in tables of axial, radial and nodal comparisons and is usually compared at the 1σ level. Note that the entire data base is used.

3.6.4.1 Axial Power Distribution Comparisons

Table 3.6.2 presents axial peak-to-average comparisons for selected statepoints from cycles 11 through 15. The following results are taken from the entire data base presented in sections 3.6.1, 3.6.2.

Simulator to measured TIP traces

Unrodded	Rodded
n = 912	n = 720
μ = 0.009	μ = 0.010
σ = 0.048	σ = 0.052

This data shows excellent agreement with other published data.

3.6.4.2 Radial Power Distribution Comparisons

Table 3.6.3 presents radial peak-to-average comparisons from selected statepoints from cycles 11 through 15. The following results were taken from the entire data base presented in Section 3.6.1, 3.6.2 and 3.6 3.

Simulator to measured TIP traces

μ = 0.001
σ = 0.043

This data shows excellent agreement to other published data.

3.6.4.3 Nodal Power Distributions Comparisons

Table 3.6.4 presents the nodal standard deviations for the 20 axial planes from the entire data base presented in Sections 3.6.1, 3.6.2.

Simulator to measured TIP traces

μ = 0.002
σ = 0.071

This data shows excellent agreement to other published data.

3.7 Delayed Neutron Parameters

This section deals with determining reliability factors for values which can be calculated but not measured. In these cases, an argument may be made for the general magnitude of the reliability factor without making direct comparisons between measured and predicted values.

The importance of the reliability of the calculated values of the delayed neutron parameters is primarily associated with the core $ß_{eff}$. The uncertainties in the calculation of $ß_{eff}$ are composed of several components, the most important of which are listed below:

a) Experimental values of ß, and λ_i by nuclide;
b) Cal ulation of the spatial nuclide inventory;
c) Ca culation of core average $ß_{eff}$ as an adjoint-flux weighted a erage over the spatial nuclide inventory.

The experimental determination of the ß's and λ's are assumed to be accurate to within 1%. The most important nuclide concentrations with respect to core ß are U^{238}, U^{235} and Pu^{239}. References 4 and 36 indicate that the uncertainty in the calculation of these parameters is about 0.3% for CASMO-3. Therefore, components a) and b) above are combined as 1.3% for CASMO-3.

The uncertainty in the calculation of a core average ß depends on the

relative adjoint-flux weighting of the individual assemblies in the core. For demonstration purposes, consider a four region core, each with a different average burnup and average ß. This is typical of advanced BWR cycles in that about a fourth of the core has seen three previous cycles, a fourth two previous cycles, a fourth one previous cycle and a fourth is the feed fuel. Typical regional ß's are given below:

Region 1 (fourth cycle fuel)	ß = 0.00543
Region 2 (third cycle fuel)	ß = 0.00581
Region 3 (second cycle fuel)	ß = 0.00633
Region 4 (feed fuel)	ß = 0.00745

The effect of errors in the calculated flux distribution can be evaluated in terms of the effect on the core average $ß_{eff}$. As a base case, weighting factors are all set to 1.0. In this case, the core average $ß_{eff}$ = 0.00626. Using a maximum error in the regional flux weighting of 7.0%, the worst error in the calculation of the core average $ß_{eff}$ is obtained by increasing the weight of the Region 1 fuel and decreasing the weight of the Region 4 fuel. It should be noted that the average relative weighting factor is unity. The revised ß is calculated as follows:

ß(1) x 1.07 = .00581
ß(2) x 1.00 = .00581
ß(3) x 1.00 = .00633
ß(4) x 0.93 = .00693
ß = .00622, which yields a -0.6% error for component c) above.

The sum of the errors for these four factors for CASMO is as follows:

1.3%(a+b) + 0.5%(c) = 1.8%

For conservatism the reliability factor for delayed neutron parameters is set at 4%.

3.8 Effective Neutron Lifetime

An argument similar to the delayed neutron parameter argument is applied to the determination of the effective neutron lifetime (Λ) uncertainty. The uncertainty components which go into the calculation of Λ are as follows:

a) Experimental values of microscopic cross sections;
b) Calculation of the spatial nuclide inventory; and
c) Calculation of the core average effective neutron life-time as an adjoint-flux weighted average over the spatial nuclide inventory.

Uncertainties for components a) and b) are assumed to be the same as described for the calculation of $ß_{eff}$, that is, 1% uncertainty in the experimental determination of nuclear cross section and .3% uncertainty in the determination of the spatial nuclide inventory for CASMO. The core average neutron lifetime depends on adjoint flux weighting of local absorption lifetimes. If a conservative estimate of the error in regional power sharing (7%) is used in determining the impact on the core average lifetime, the error in lifetime is on the order of 1.0%. Combining all of these uncertainties linearly results in a total uncertainty of 1.8% for CASMO-3. Therefore, a 4% reliability factor will be applied to the neutron lifetime calculation when applied to safety related calculations.

Table 3.6.1 Full Power Statepoints

Cycle	Cycle Exposure (GWD/MTU)	Power (%)	Rod Density (%)	k_{eff}
11	.388	99.9	11.71	0.9989
	.819	100.0	8.26	0.9981
	1.331	99.9	8.75	0.9980
	1.759	100.0	7.85	0.9981
	2.251	100.0	7.71	0.9981
	2.659	100.0	7.61	0.9983
	3.223	100.0	7.37	0.9985
	3.716	100.0	7.30	0.9980
	4.128	100.1	7.23	0.9987
	4.631	100.0	6.71	0.9990
	5.301	99.9	4.58	1.0003
	5.624	100.0	4.17	1.0009
	6.352	98.6	0.03	1.0017
	6.756	92.1	0.03	1.0016
	7.256	83.5	0.03	1.0015
	7.764	74.0	0.03	1.0014
	8.159	66.4	0.03	1.0016
12	0.535	100.0	2.89	1.0006
	1.063	100.0	3.17	0.9994
	1.736	99.9	5.23	0.9988
	1.945	99.9	5.23	0.9993
	2.478	99.9	7.82	0.9992
	2.858	100.0	7.30	0.9998
	4.497	99.9	7.02	1.0000
	4.880	99.9	5.54	0.9998
	5.478	99.8	3.03	1.0002
	6.830	95.7	0.96	1.0004
	7.148	91.1	0.00	0.9999
13	0.783	100.0	7.58	0.9963
	1.408	100.0	8.26	0.9956
	2.149	100.0	9.09	0.9952
	2.672	100.0	10.47	0.9961
	3.351	100.0	10.74	0.9959
	3.967	99.9	10.47	0.9965
	4.956	99.9	8.26	0.9966
	6.165	100.0	6.06	0.9973
	6.707	100.0	3.58	0.9976
	7.373	99.9	0.00	0.9975
	8.229	86.8	0.00	0.9970
	8.724	77.8	0.00	0.9968
	9.103	70.6	0.00	0.9969
	9.729	58.9	0.00	0.9969
	10.165	50.9	0.00	0.9968
14	0.751	100.0	6.20	0.9970
	1.296	100.1	6.37	0.9962
	1.977	100.0	7.02	0.9955
	2.648	100.1	8.26	0.9958
	3.325	100.1	8.68	0.9956
	4.170	99.9	8.68	0.9962
	5.284	100.1	8.75	0.9970
	5.904	100.0	6.61	0.9969
	6.530	100.0	4.58	0.9983
	7.454	100.0	1.89	0.9992
	8.237	92.7	0.00	0.9990
	8.882	82.5	0.00	0.9988

Table 3.6.1 Full Power Statepoints (Continued)

Cycle	Cycle Exposure (GWD/MTU)	Power (%)	Rod Density (%)	k_{eff}
15	0.187	99.8	7.51	0.9979
	0.954	99.9	6.23	0.9963
	1.790	99.8	7.92	0.9958
	2.735	99.8	8.68	0.9947
	3.591	99.7	8.95	0.9943
	4.518	99.7	9.54	0.9944
	5.409	99.7	9.33	0.9959
	6.802	99.8	8.13	0.9971
	7.636	99.8	6.30	0.9971
	8.349	99.5	5.51	0.9977
	9.332	99.7	2.86	0.9982
	10.301	91.1	1.10	0.9972
	11.197	73.4	0.00	0.9960

Table 3.6.2 Axial Power Distribution Comparison

Cycle	Location	Rod	Peak to Average TIP	Peak to Average Calculated	% Difference
11	20-29	Out	1.185	1.143	3.5
11	28-13	Out	1.272	1.297	-2.0
12	28-29	Out	1.241	1.255	-1.1
12	20-21	Out	1.182	1.192	-0.8
12	12-21	Out	1.183	1.194	-1.0
13	44-29	Out	1.405	1.406	-0.1
13	12-29	Out	1.438	1.393	3.1
13	28-21	Out	1.155	1.163	-0.6
14	20-29	Out	1.318	1.302	1.2
14	44-29	Out	1.256	1.231	1.9
14	12-37	Out	1.289	1.275	1.1
15	36-29	Out	1.161	1.193	-2.8
15	36-37	Out	1.415	1.326	6.3
15	12-37	Out	1.361	1.349	0.9
11	20-37	In	1.611	1.598	0.8
12	20-21	In	1.225	1.259	-2.7
13	28-45	In	1.173	1.115	5.0
14	20-37	In	1.500	1.434	4.4
14	12-29	In	1.324	1.333	-0.6
15	28-29	In	1.195	1.181	1.1

Table 3.6.3 Radial Power Distribution Comparisons

Cycle	Location	Exposure	TIP	Calculated	% Difference
11	20-37	0.388	1.118	1.103	1.4
11	36-13	1.331	1.151	1.185	-3.0
11	28-37	2.251	1.179	1.157	1.9
11	20-29	3.223	1.141	1.122	1.7
11	12-21	4.631	1.230	1.242	-1.0
11	12-29	7.764	1.228	1.176	4.2
12	36-29	1.063	1.159	1.139	1.7
12	36-29	2.478	1.187	1.150	3.1
12	12-21	4.880	1.155	1.131	2.1
12	28-21	6.830	1.131	1.199	-6.1
12	28-29	6.830	1.190	1.208	-1.6
12	28-37	7.148	1.159	1.208	-4.2
13	20-21	2.150	1.217	1.278	-5.0
13	28-37	2.672	1.136	1.149	-1.2
13	36-29	6.165	1.117	1.150	-3.0
13	36-29	6.707	1.125	1.147	-1.9
13	28-21	7.374	1.155	1.163	-0.7
13	28-37	10.165	1.120	1.127	-0.6
14	12-29	1.297	1.129	1.144	-1.3
14	36-29	1.977	1.117	1.168	-4.5
14	20-37	3.325	1.153	1.121	2.7
14	28-21	5.904	1.121	1.130	-0.8
14	28-13	7.454	1.110	1.130	-1.8
14	20-37	8.882	1.181	1.193	-1.0
15	12-29	0.954	1.111	1.168	-5.2
15	36-13	2.735	1.181	1.157	2.0
15	28-21	5.409	1.148	1.118	2.7
15	20-37	8.349	1.168	1.151	1.5
15	36-21	10.301	1.140	1.199	-5.2
15	20-37	11.197	1.233	1.201	2.6

Table 3.6.4 Power Distribution Standard Deviations in 20 Axial Planes

Planes	Planar Standard Deviation
3	0.062
4	0.061
5	0.056
6	0.054
7	0.055
8	0.054
9	0.056
10	0.060
11	0.058
12	0.060
13	0.062
14	0.064
15	0.062
16	0.060
17	0.066
18	0.061
19	0.060
20	0.062
21	0.063
22	0.074

Figure 3.6.1 Measured and Calculated Detector Responses BOC Cycle 11

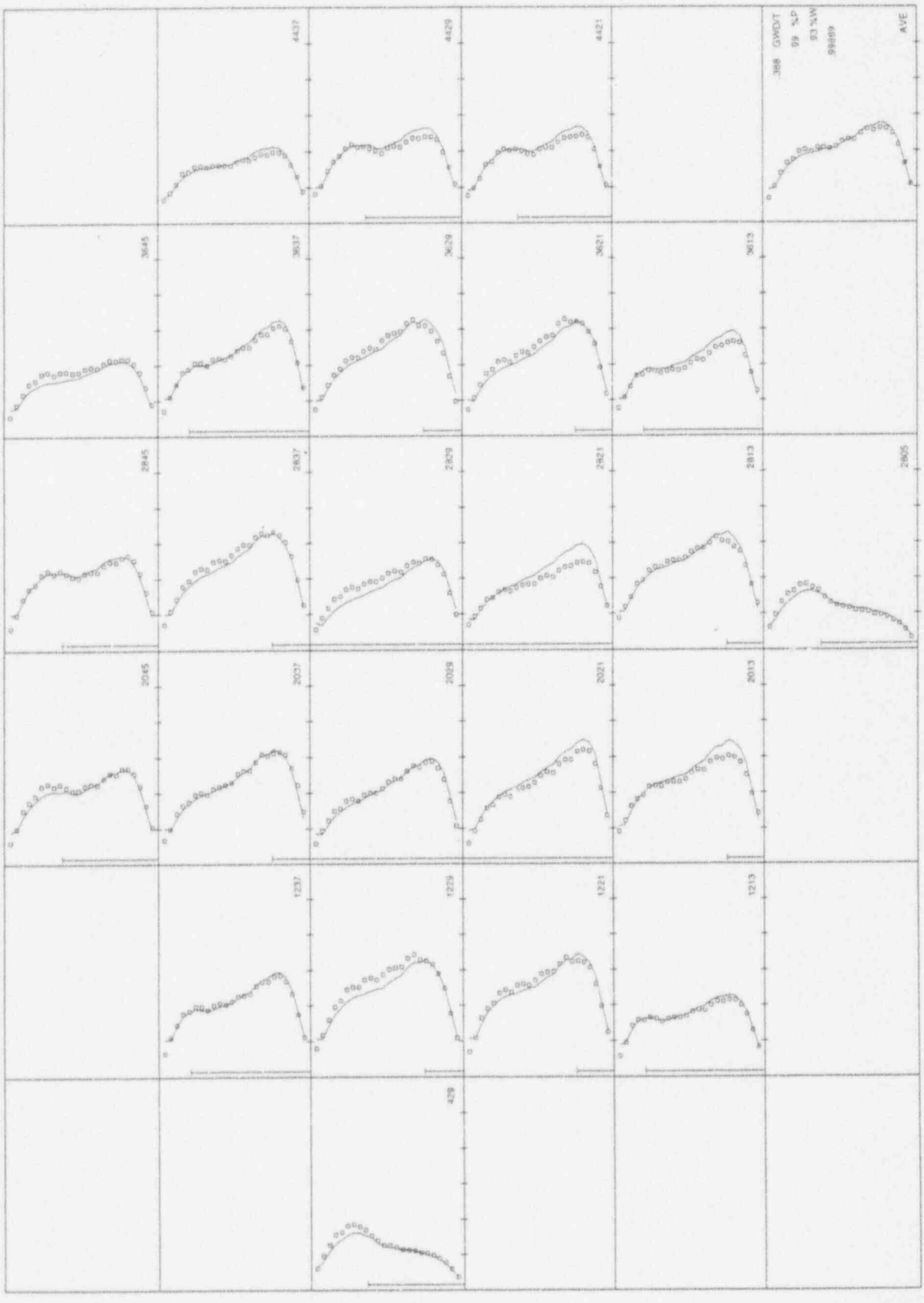

Figure 3.6.2 Measured and Calculated Detector Responses MOC Cycle 11

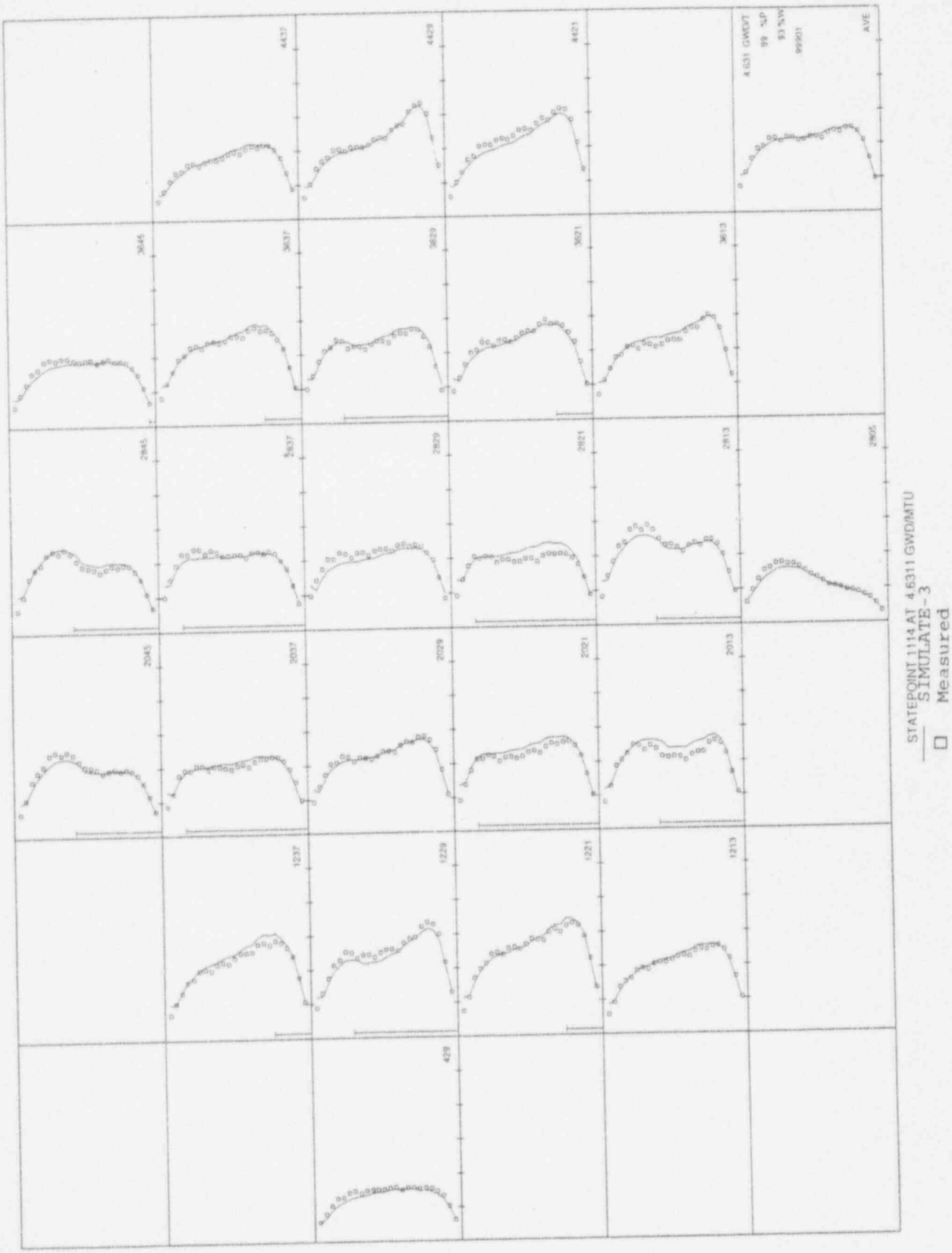

Figure 3.6.3 Measured and Calculated Detector Responses EOC Cycle 11

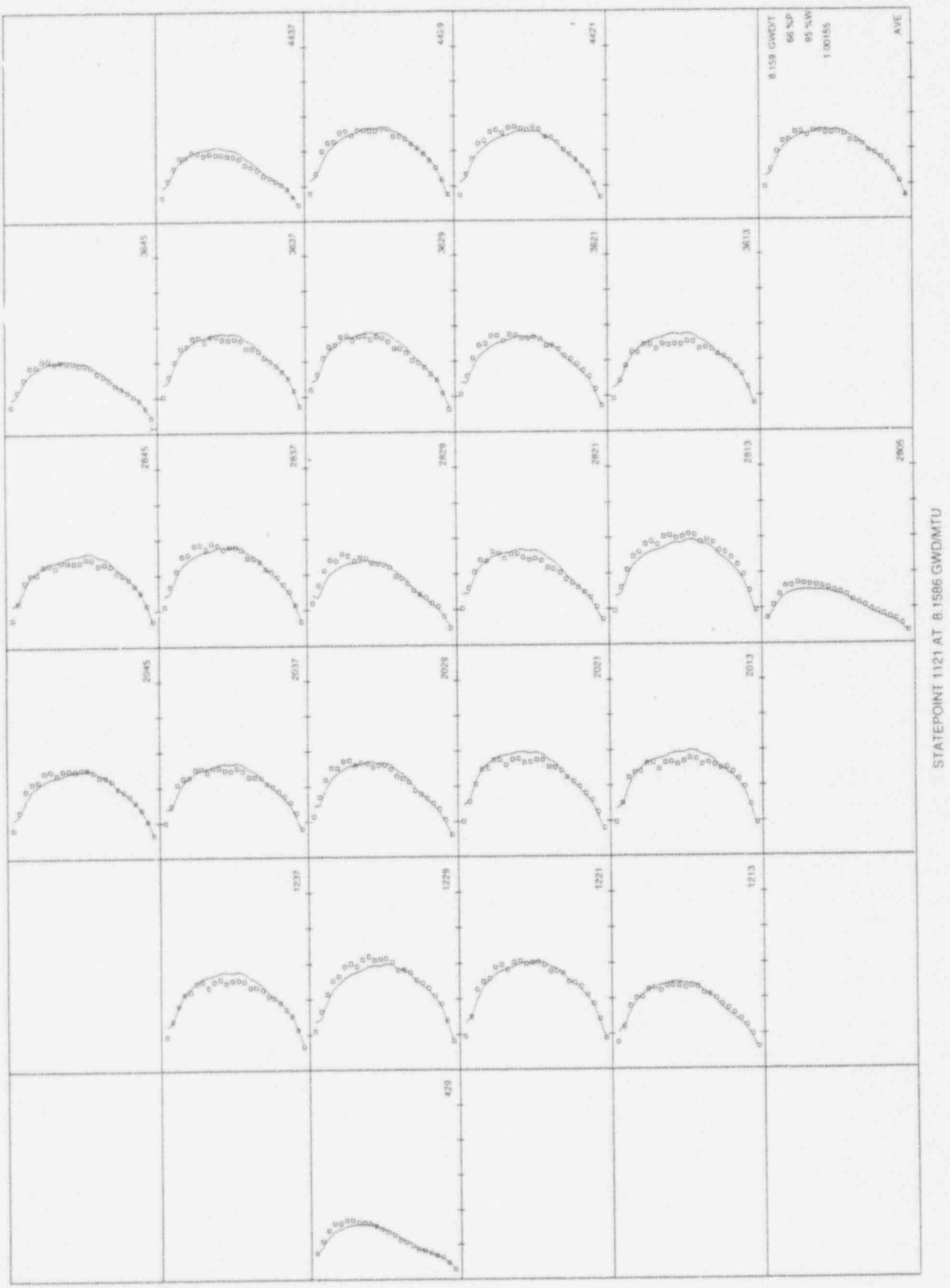

Figure 3.6.4 Measured and Calculated Detector Responses BOC Cycle 12

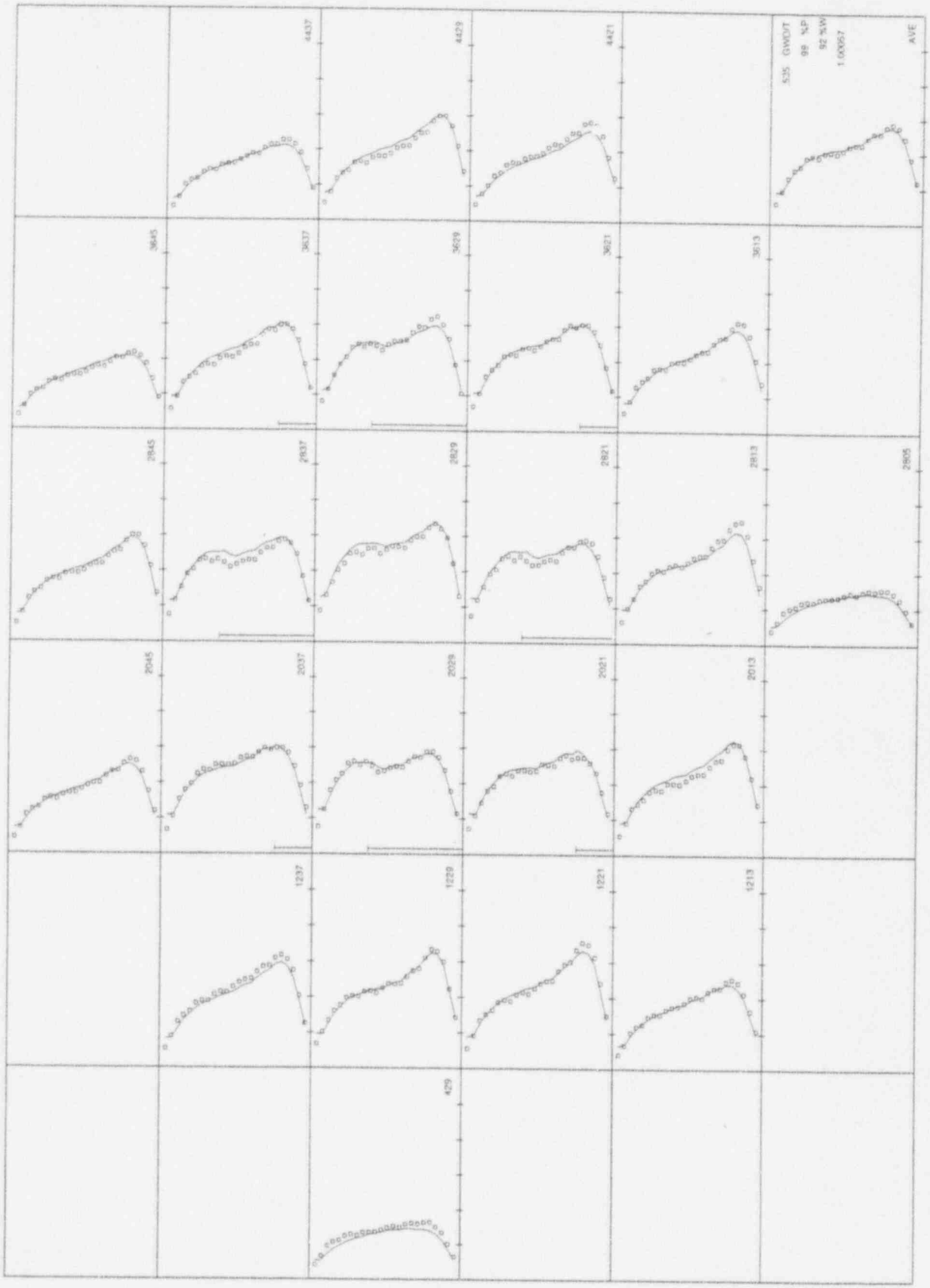

Figure 3.6.5 Measured and Calculated Detector Responses MOC Cycle 12

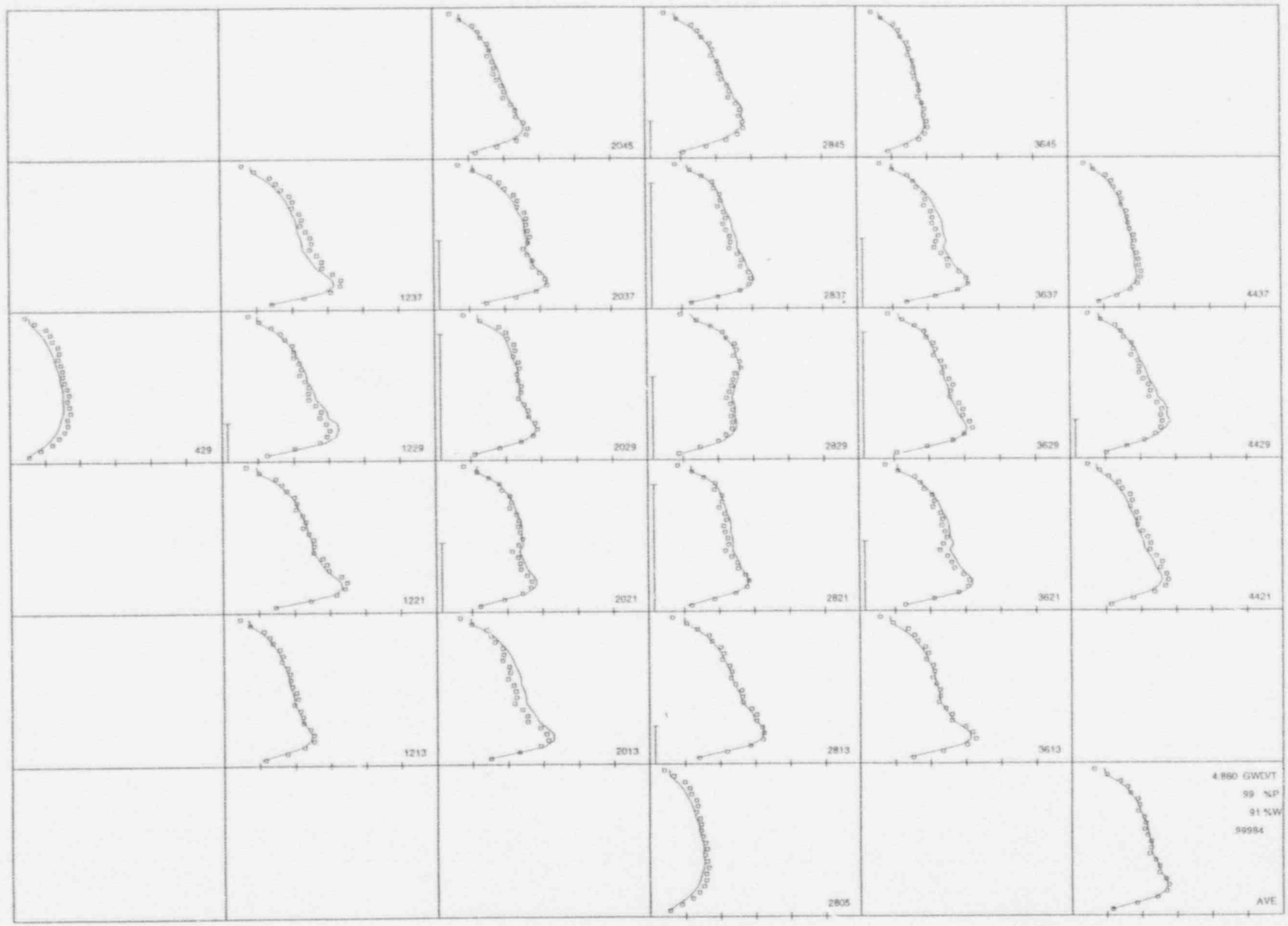

STATEPOINT 1208 AT 4.8804 GWD/MTU

SIMULATE-3

Measured

Figure 3.6.6 Measured and Calculated Detector Responses EOC Cycle 12

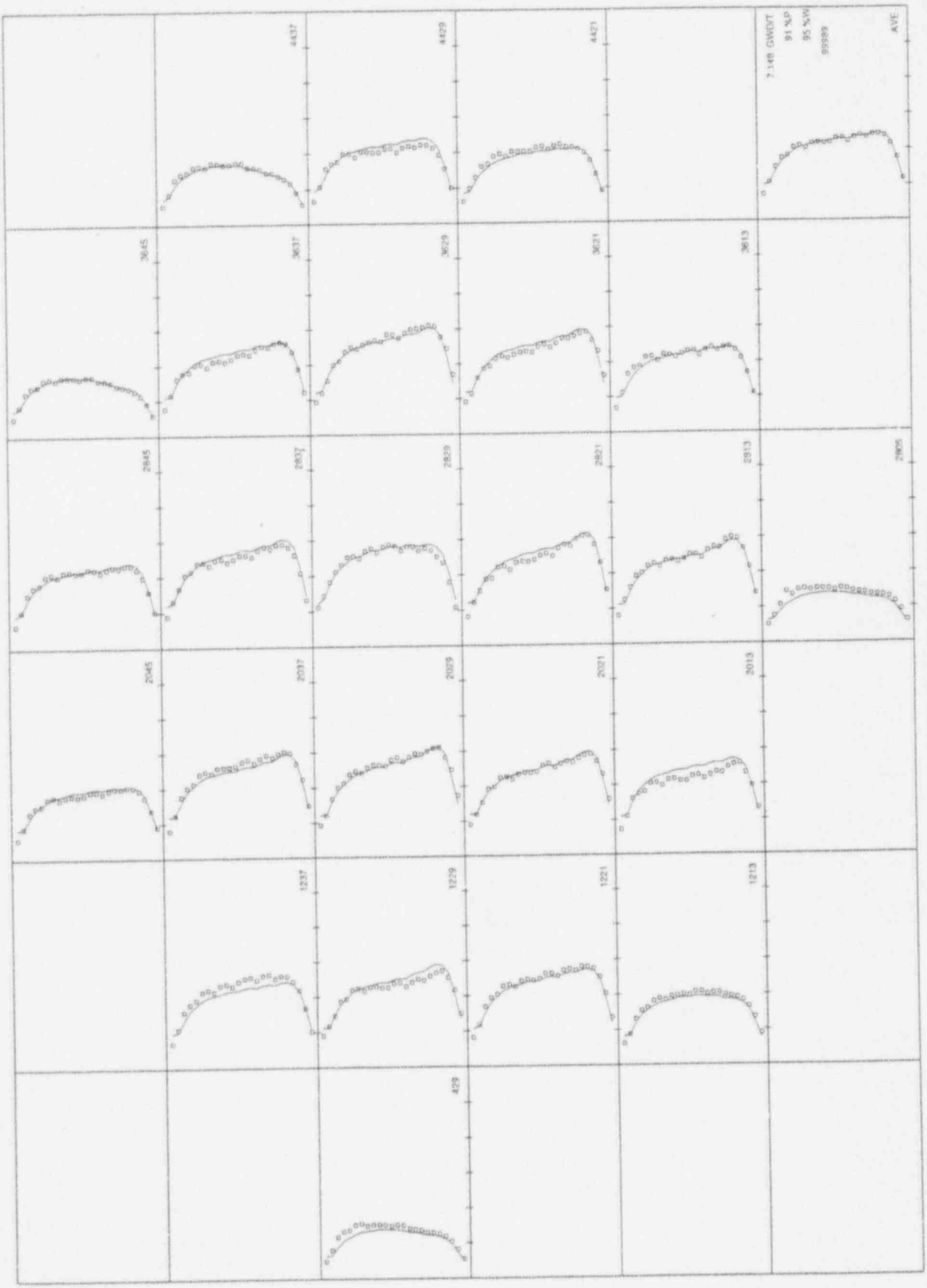

Figure 3.6.7 Measured and Calculated Detector Responses BOC Cycle 13

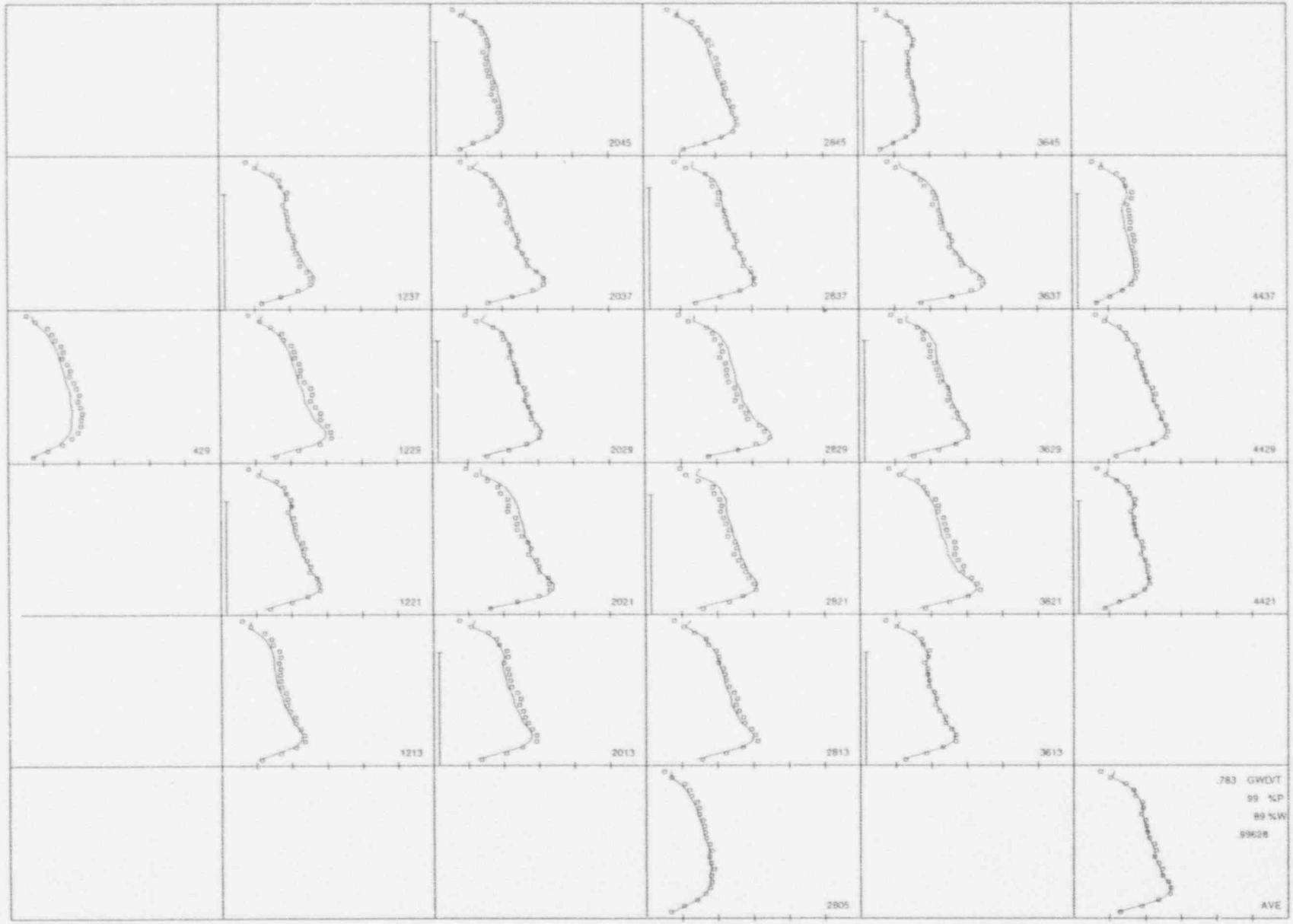

STATEPOINT 1301 AT 0.785 GWD/MTU

SIMULATE-3
Measured

Figure 3.6.8 Measured and Calculated Detector Responses MOC Cycle 13

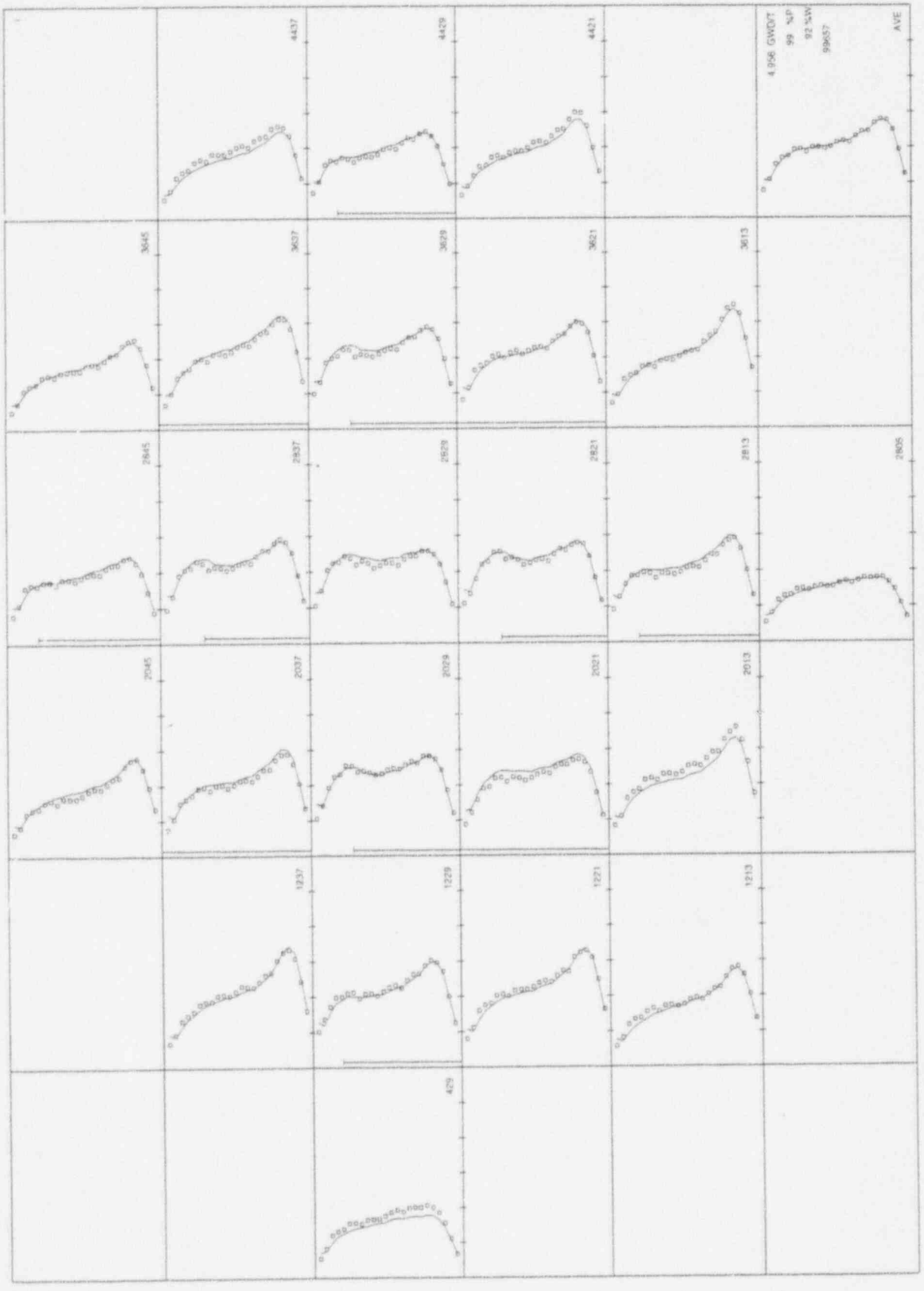

Figure 3.6.9 Measured and Calculated Detector Responses EOC Cycle 13

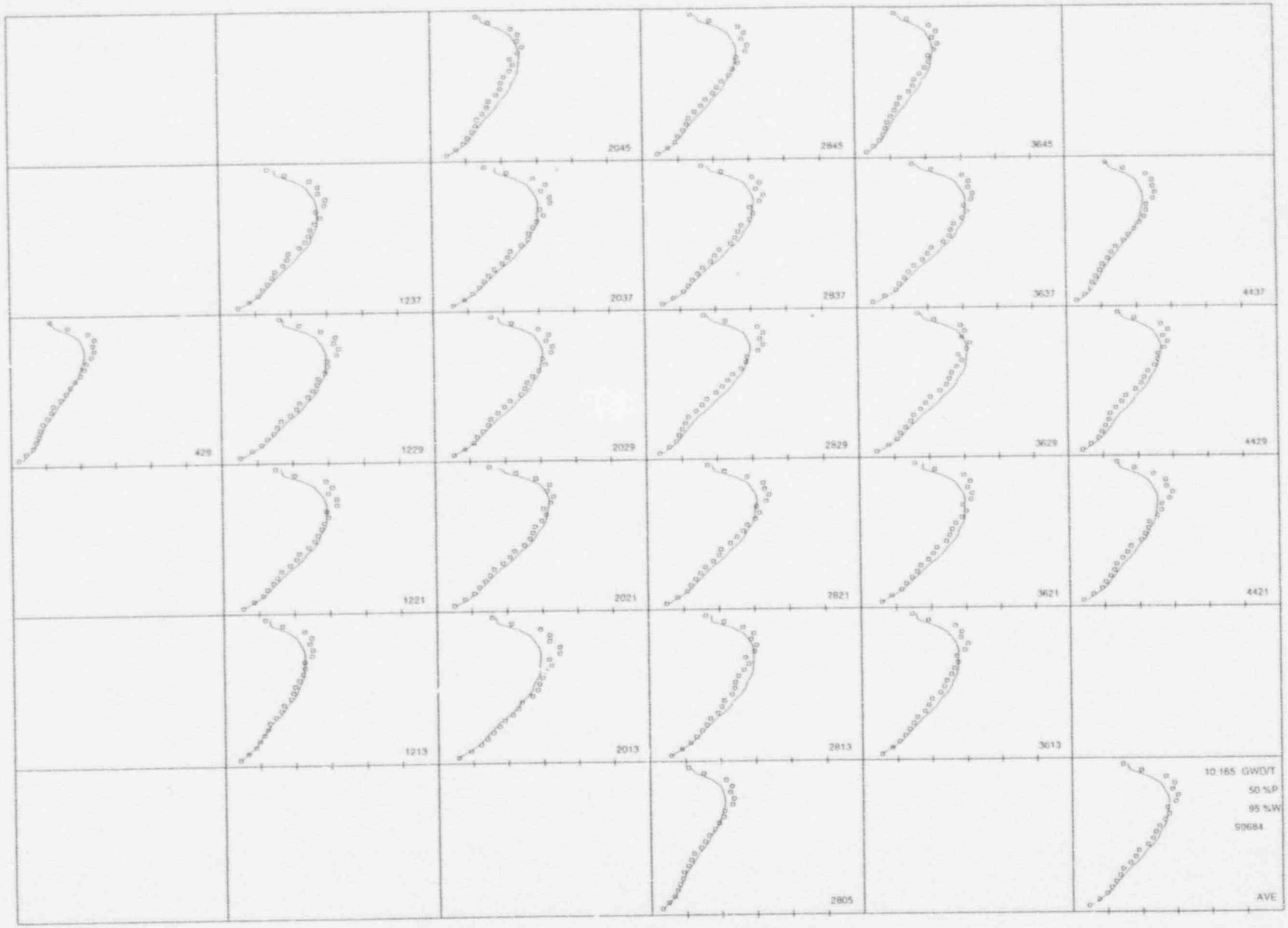

STATEPOINT 1318 AT 10.1651 GWD/MTU

SIMULATE-3
Measured

Figure 3.6.10 Measured and Calculated Detector Responses BOC Cycle 14

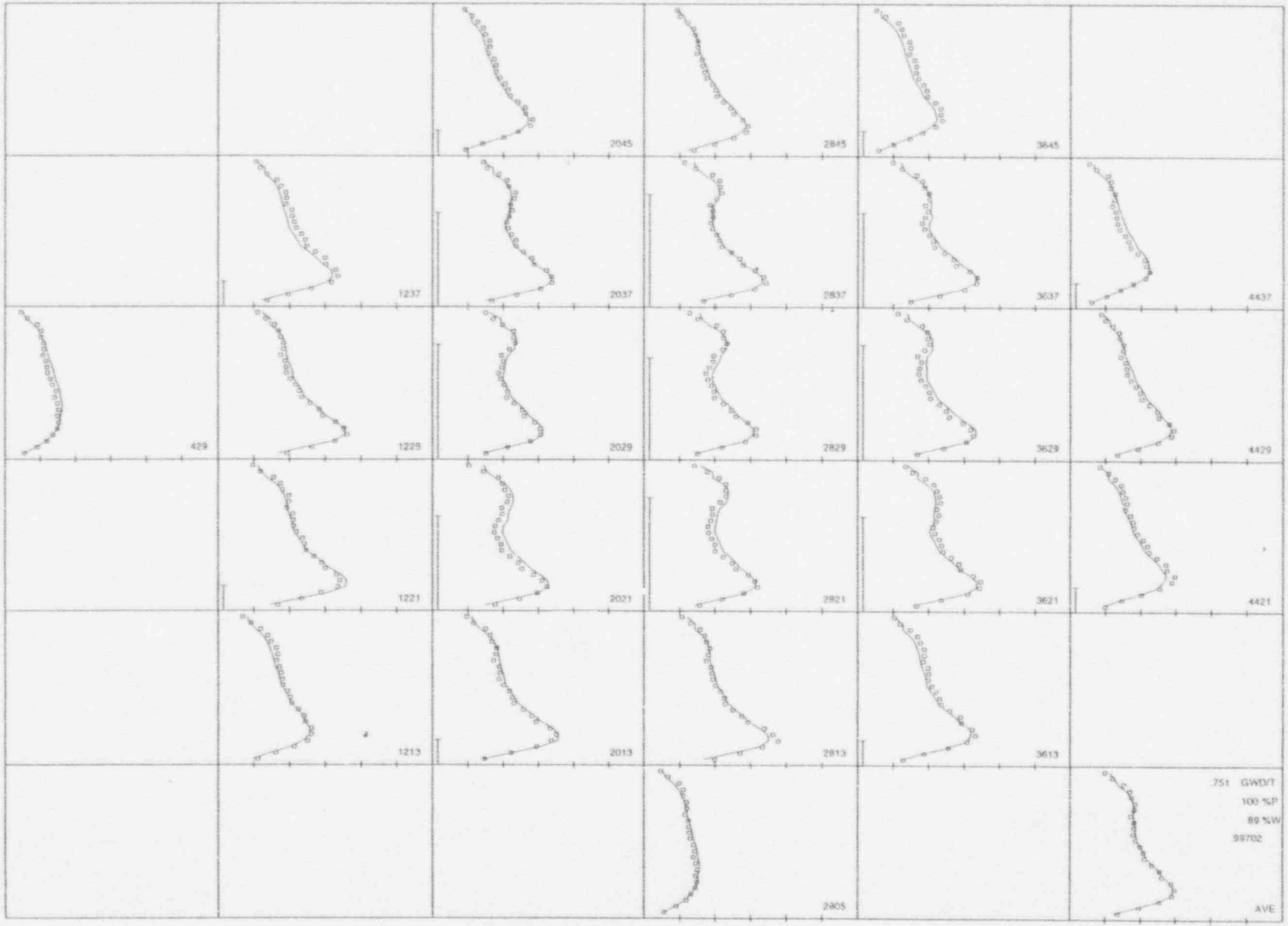

STATEPOINT 1401 AT 0.7510 GWD/MTU

SIMULATE-3
Measured

Figure 3.6.11 Measured and Calculated Detector Responses MOC Cycle 14

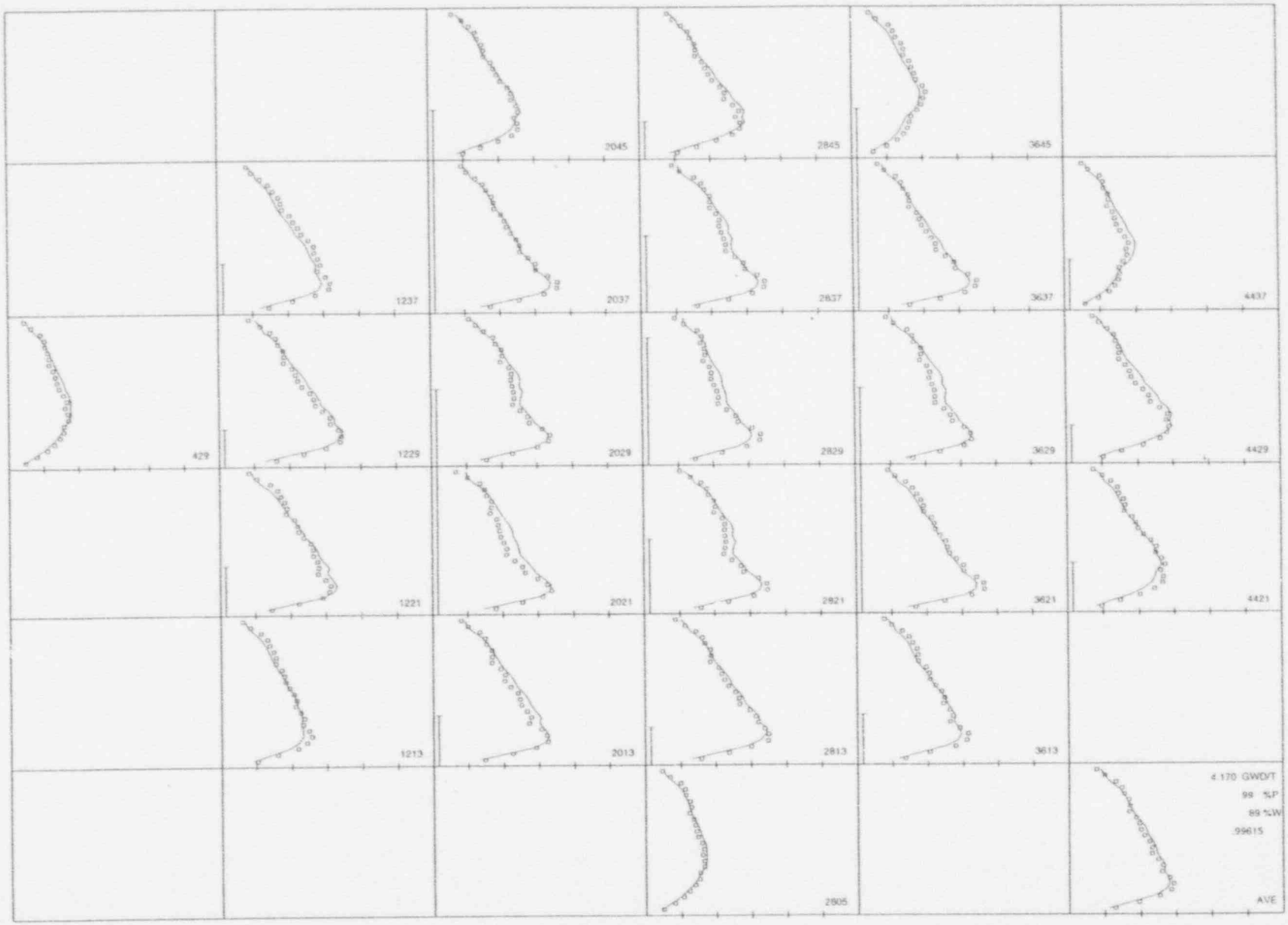

STATEPOINT 1406 AT 4.1703 GWD/MTU

SIMULATE-3
Measured

Figure 3.6.12 Measured and Calculated Detector Responses EOC Cycle 14

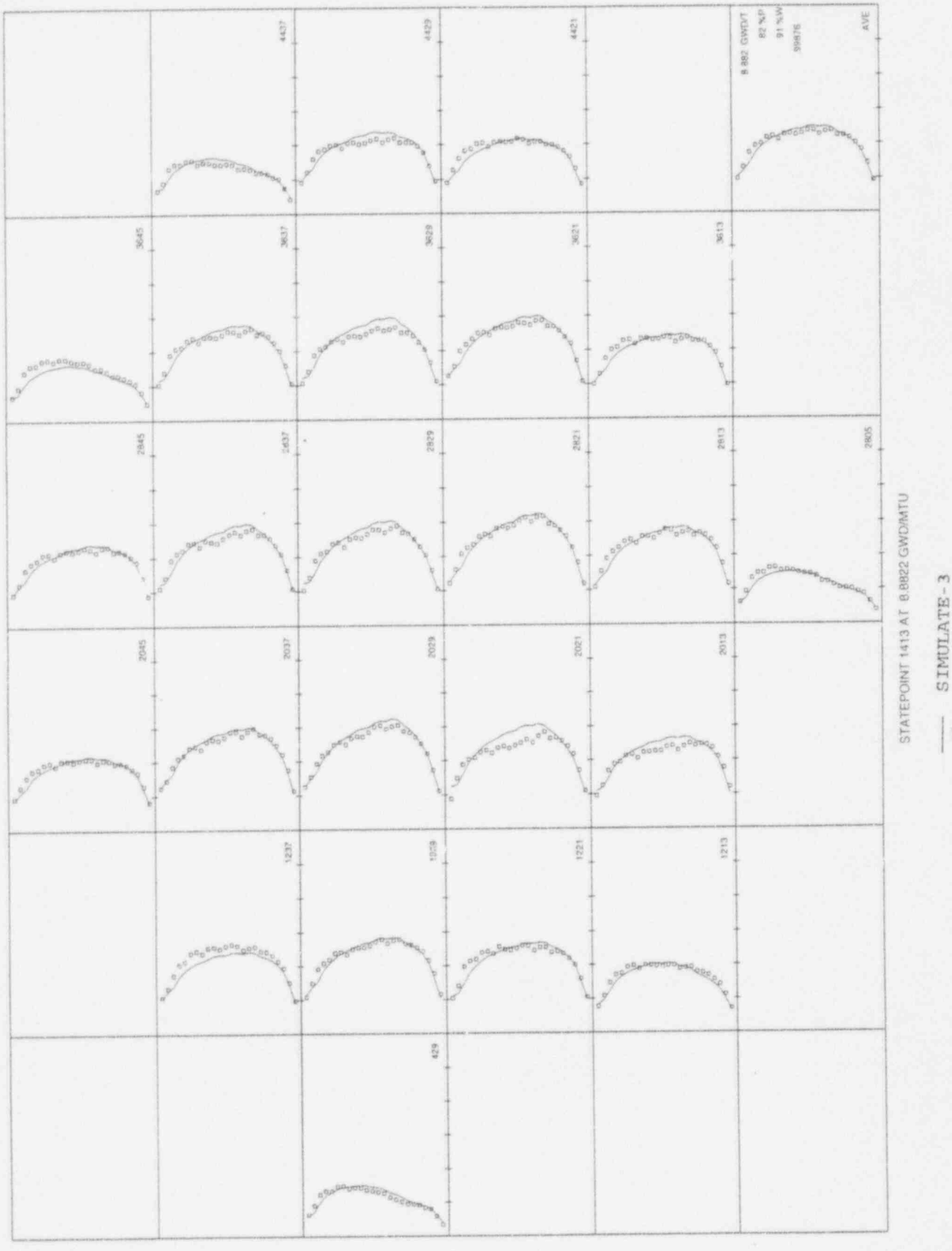

Figure 3.6.13 Measured and Calculated Detector Responses BOC Cycle 15

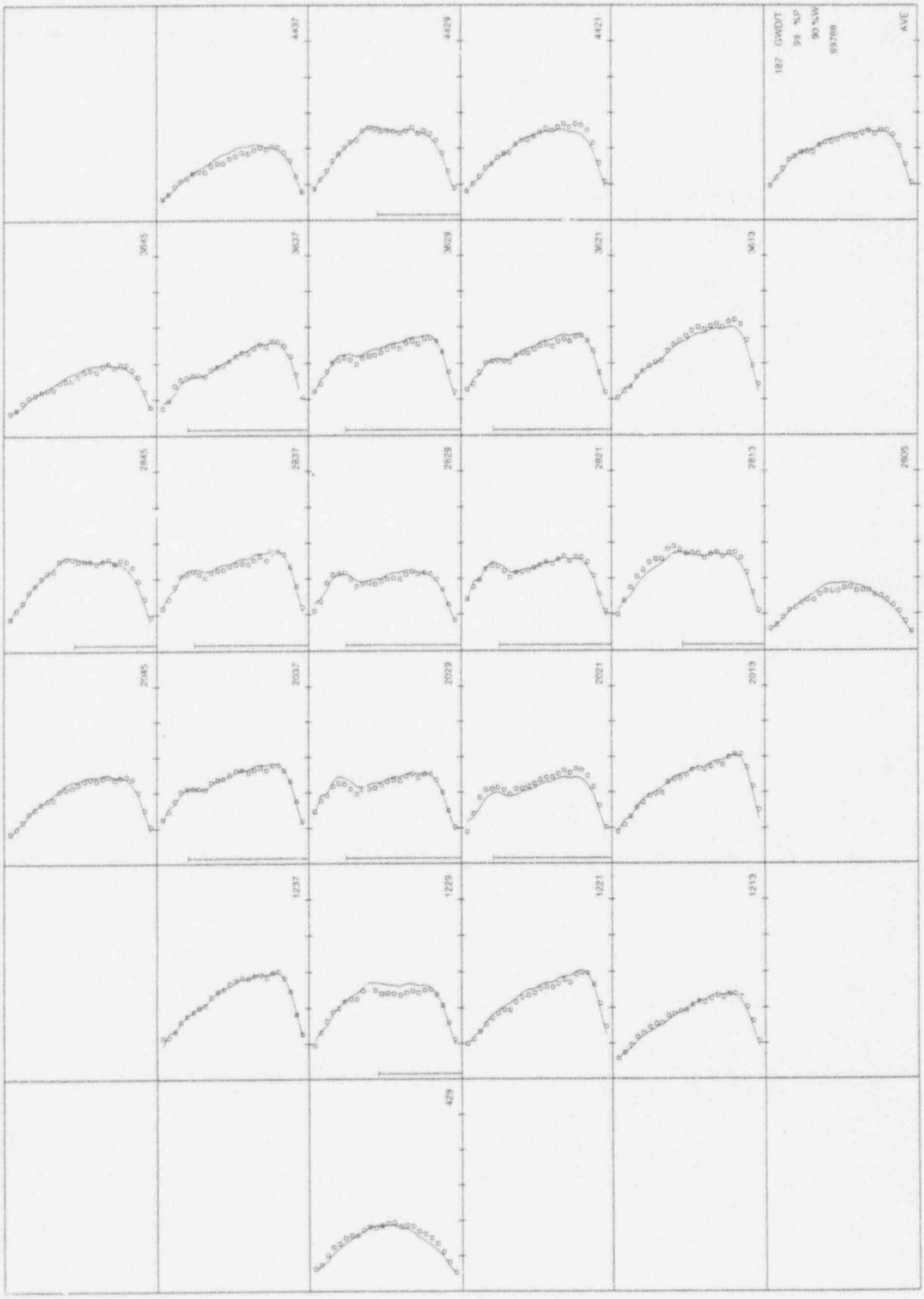

Figure 3.6.14 Measured and Calculated Detector Responses MOC Cycle 15

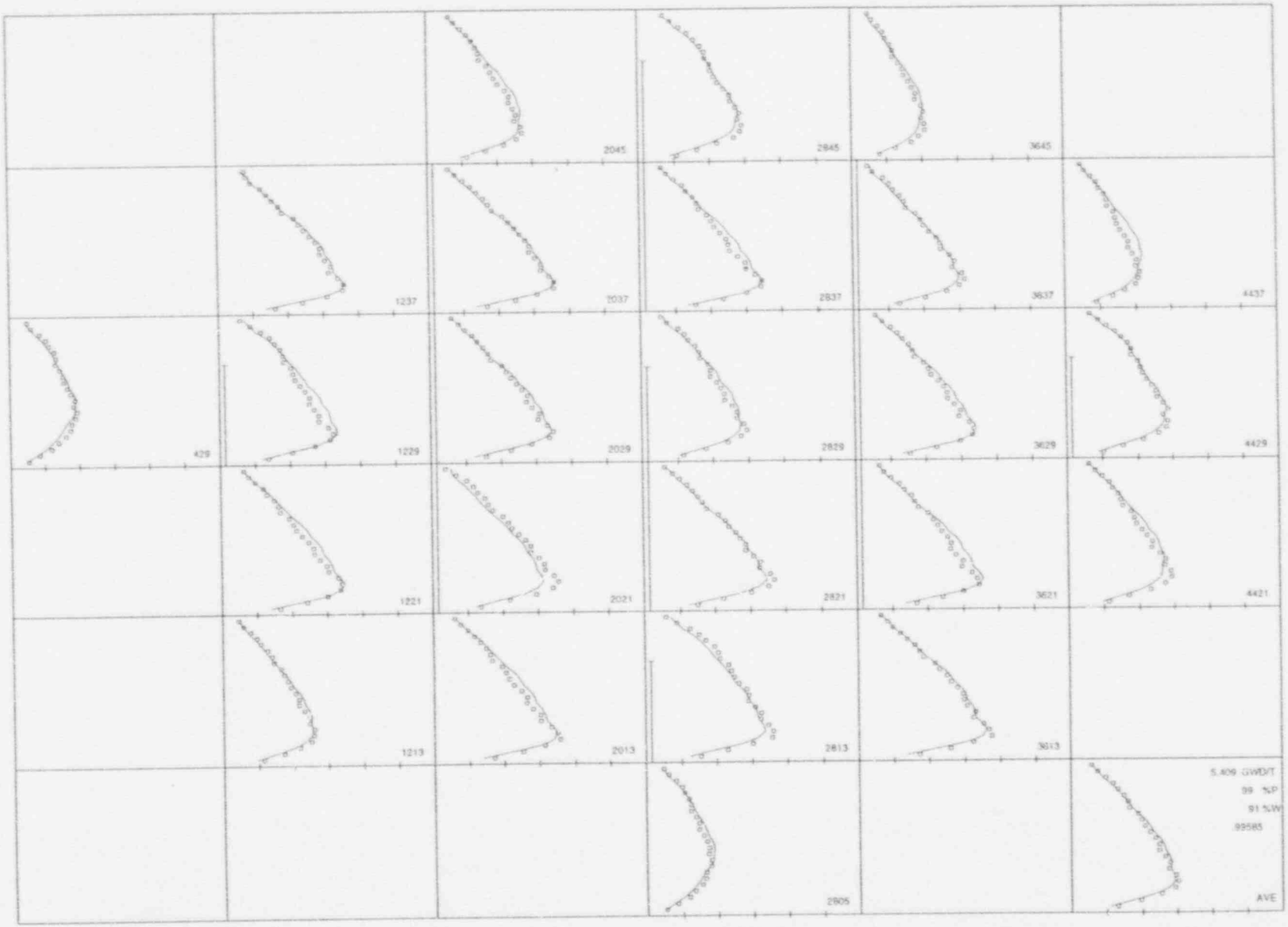

STATEPOINT 1507 AT 5.4086 GWD/MTU

SIMULATE-3
Measured

Figure 3.6.15 Measured and Calculated Detector Responses EOC Cycle 15

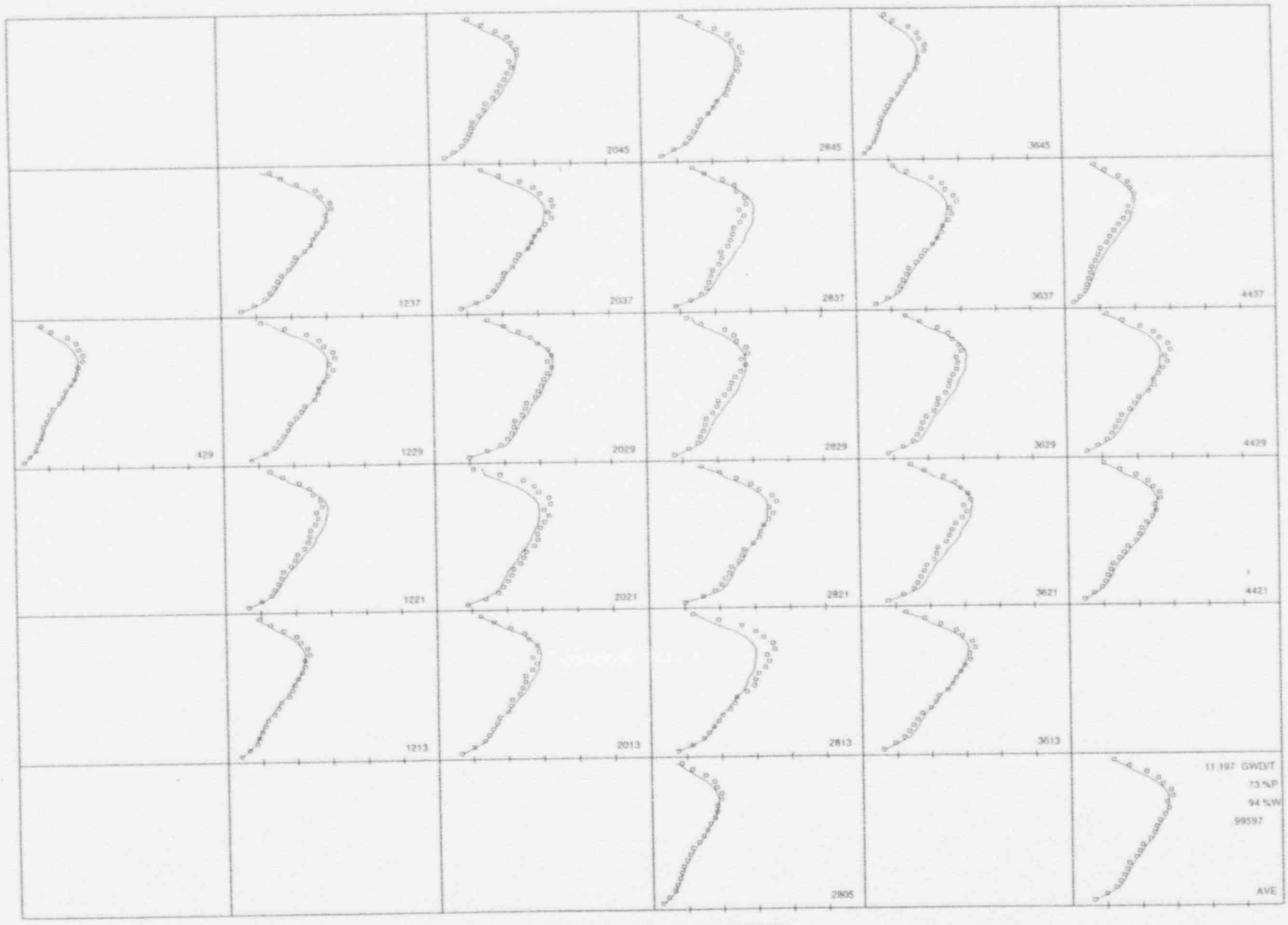

STATEPOINT 1513 AT 11.1967 GWD/MTU

—— SIMULATE-3
□ Measured

Figure 3.6.16

Observed Differences Density Function Comparison

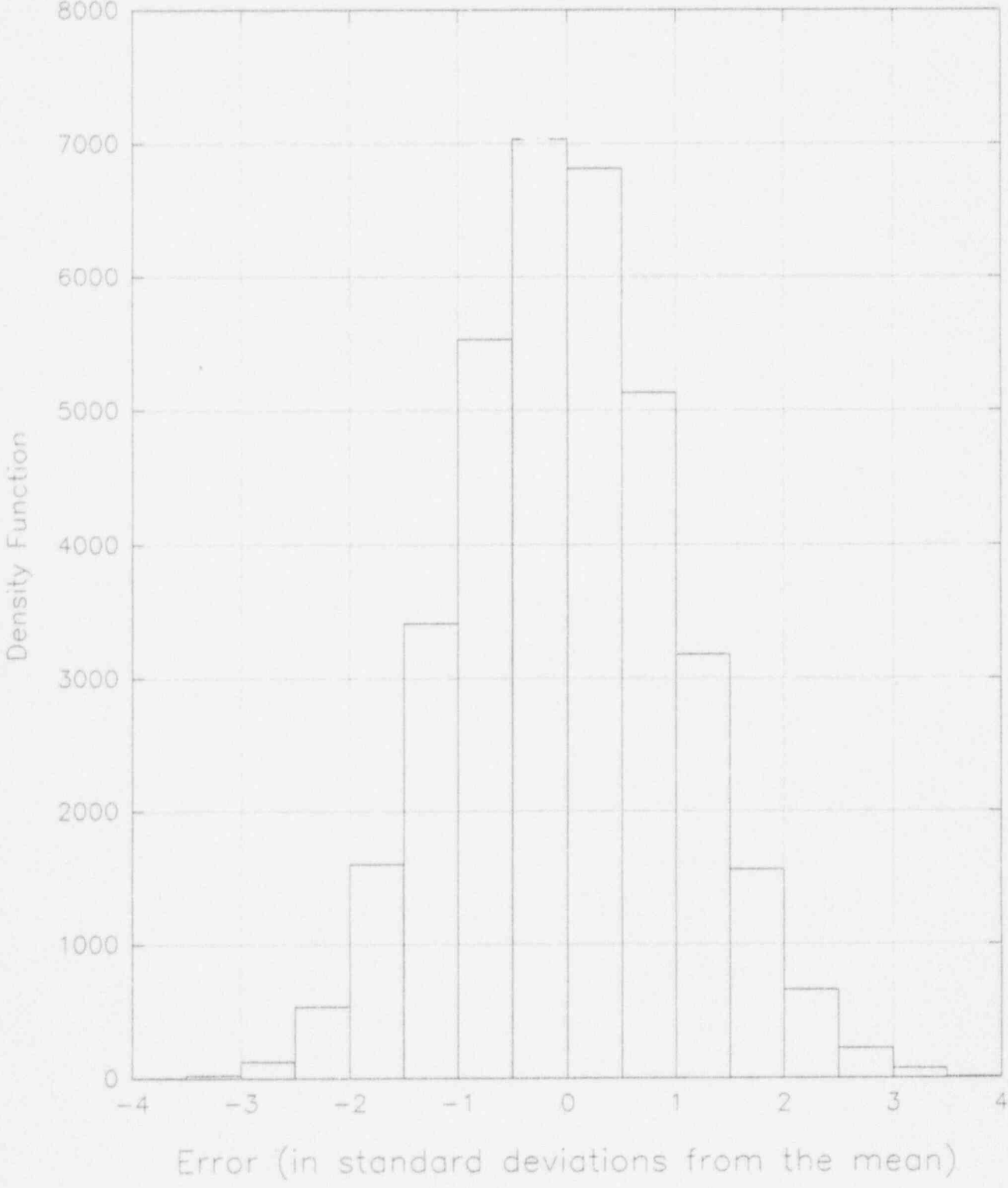

Figure 3.6.17

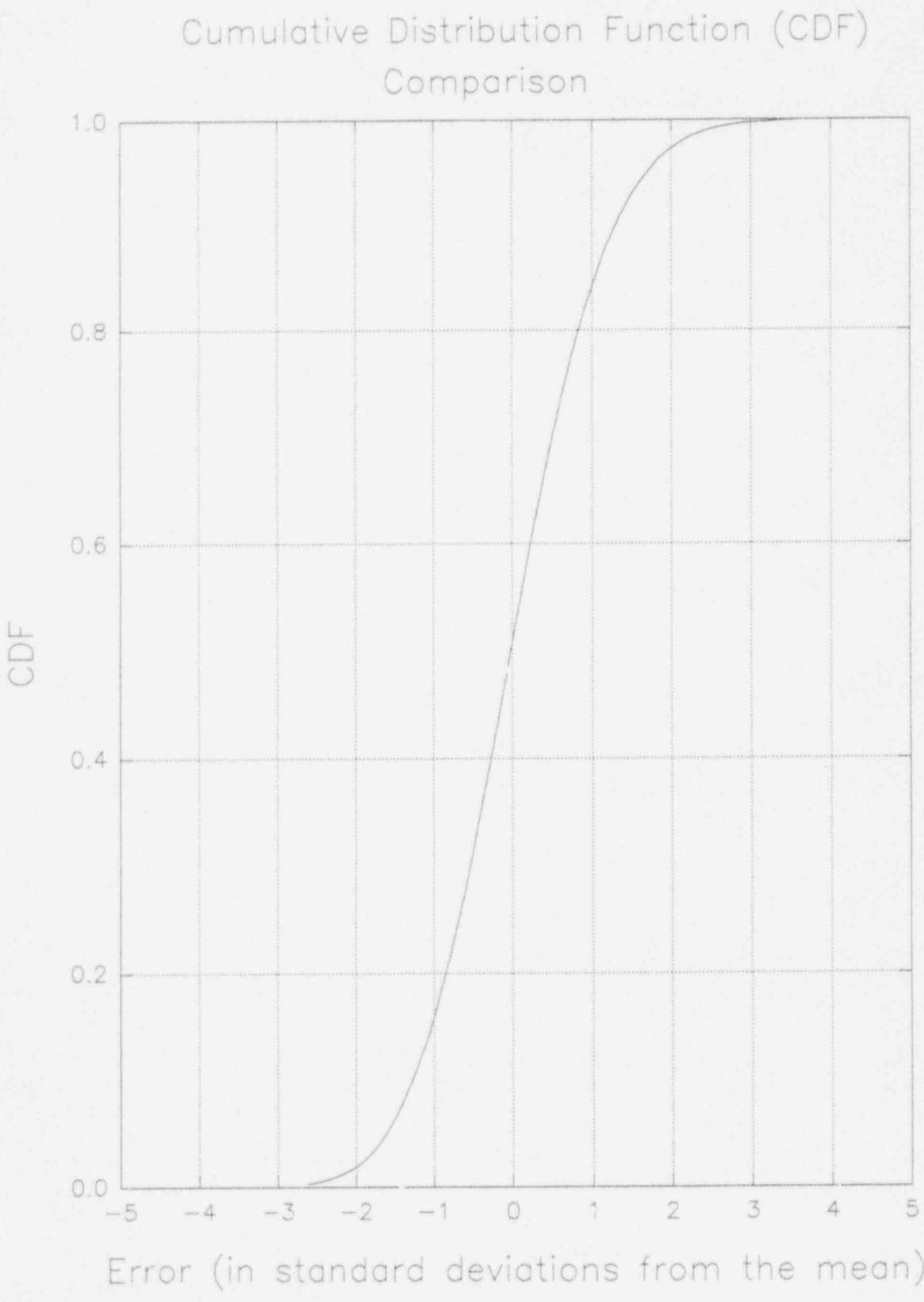
Cumulative Distribution Function (CDF)
Comparison
1.0
0.8
0.6
0.4
0.2
0.0
CDF
−5
−4
−3
−2
−1
0
1
2
3
4
5
Error (in standard deviations from the mean)

Figure 3.6.18

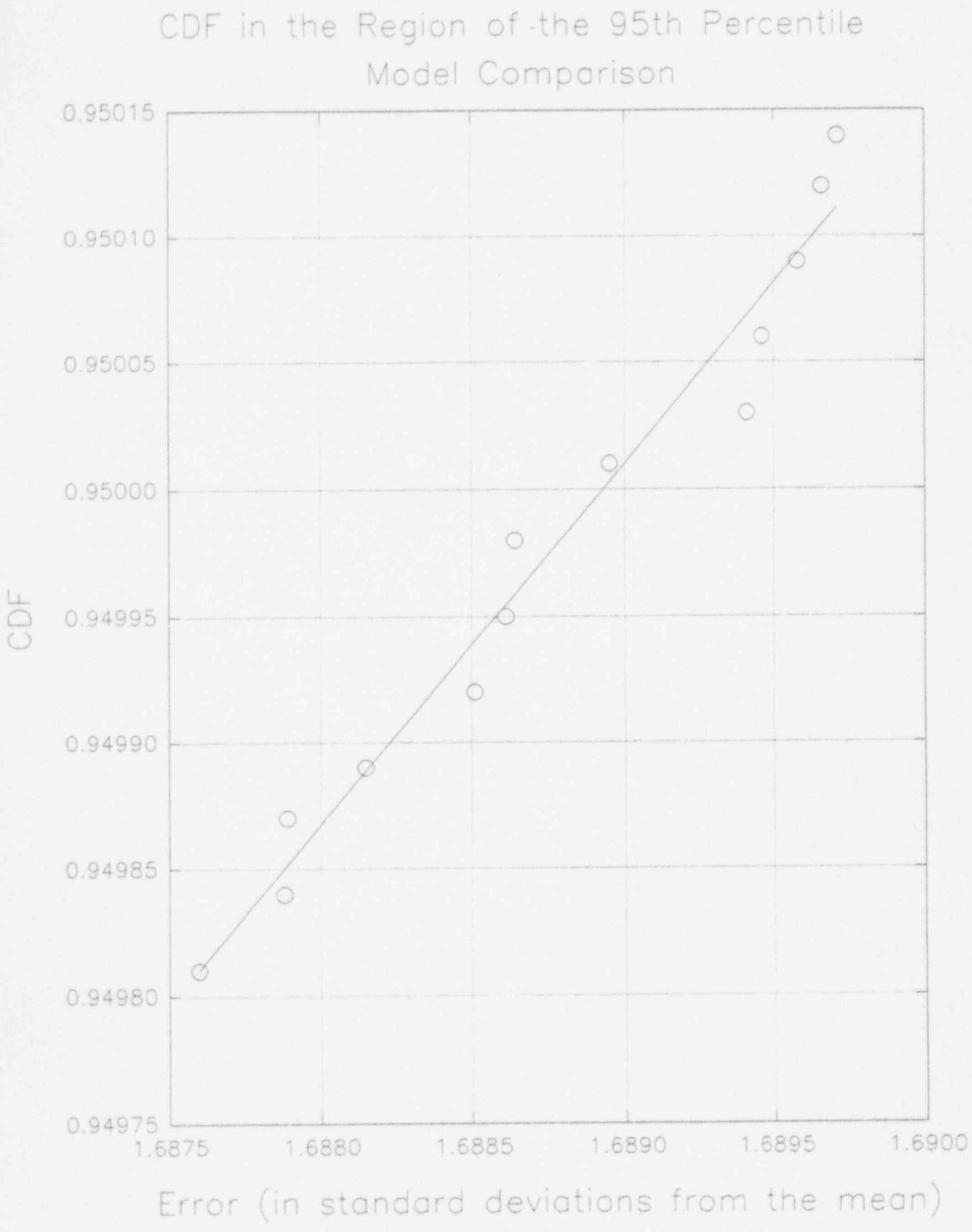
CDF in the Region of the 95th Percentile
Model Comparison
0.95015
0.95010
0.95005
0.95000
0.94995
0.94990
0.94985
0.94980
0.94975
CDF
1.6875
1.6880
1.6885
1.6890
1.6895
1.6900
Error (in standard deviations from the mean)

Figure 3.6.19

Observed Differences Density Function
Integrated Reaction Rates Comparison

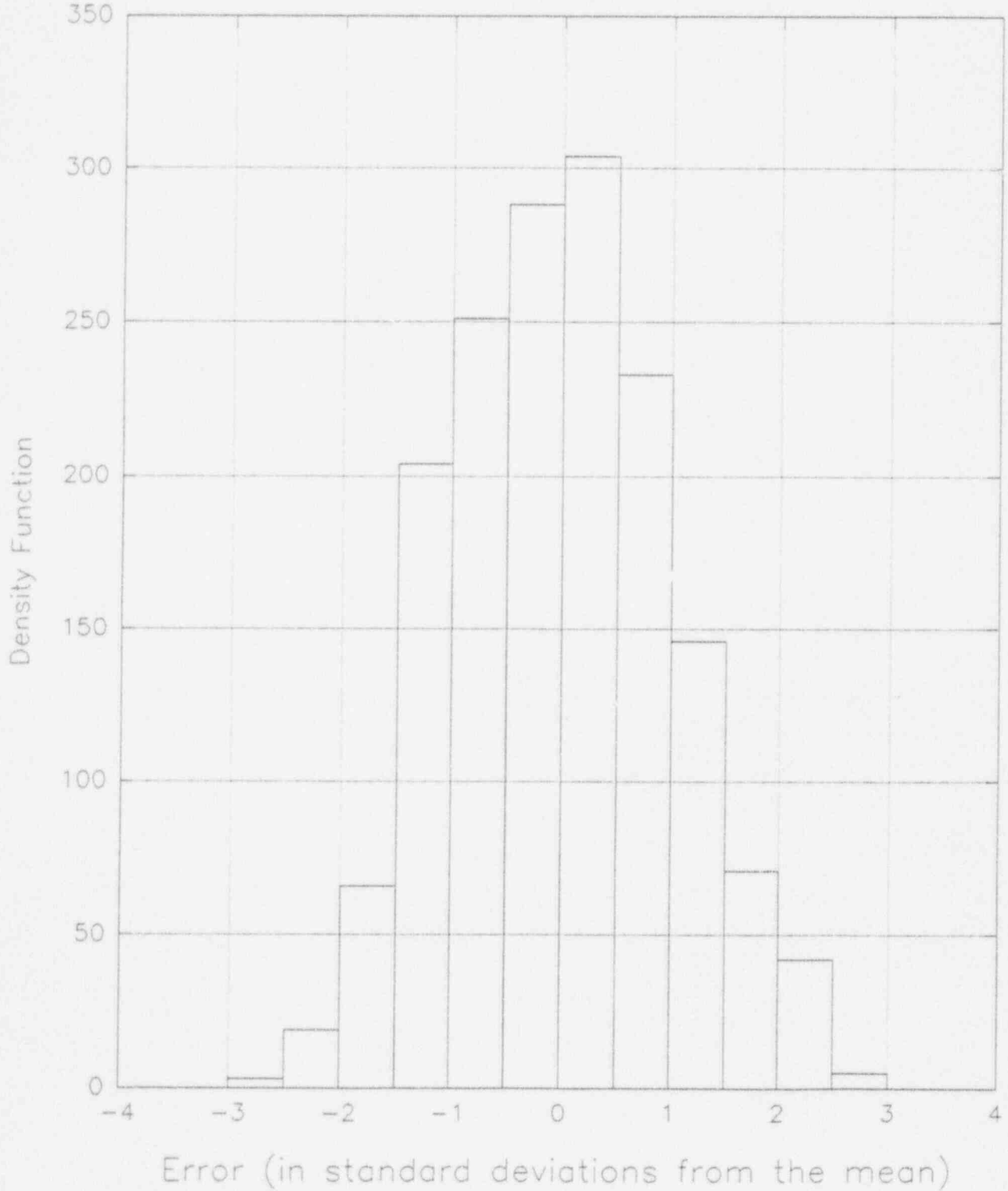

Figure 3.6.20

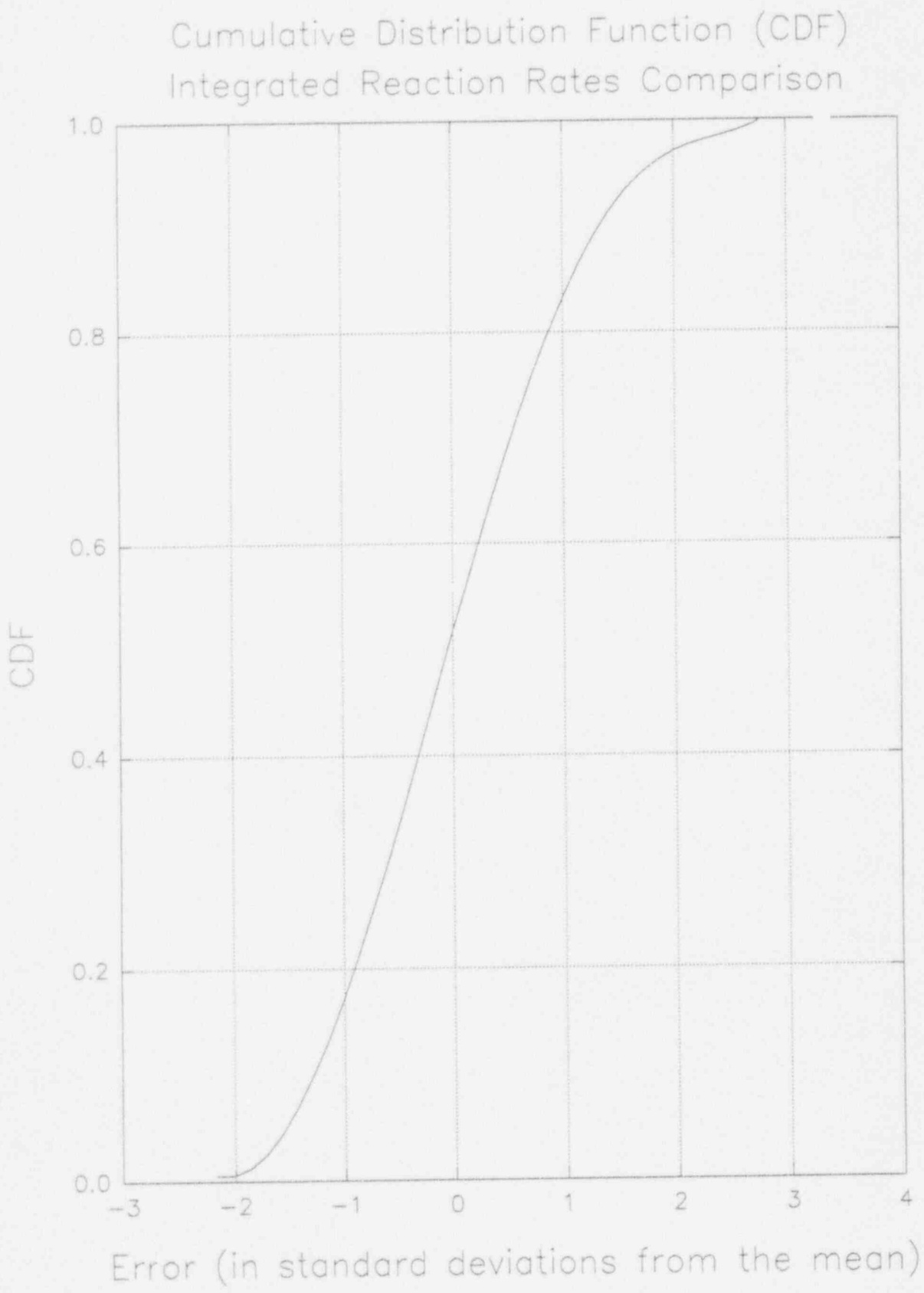
Cumulative Distribution Function (CDF)
Integrated Reaction Rates Comparison
CDF
1.0
0.8
0.6
0.4
0.2
0.0
−3
−2
−1
0
1
2
3
4
Error (in standard deviations from the mean)

Figure 3.6.21

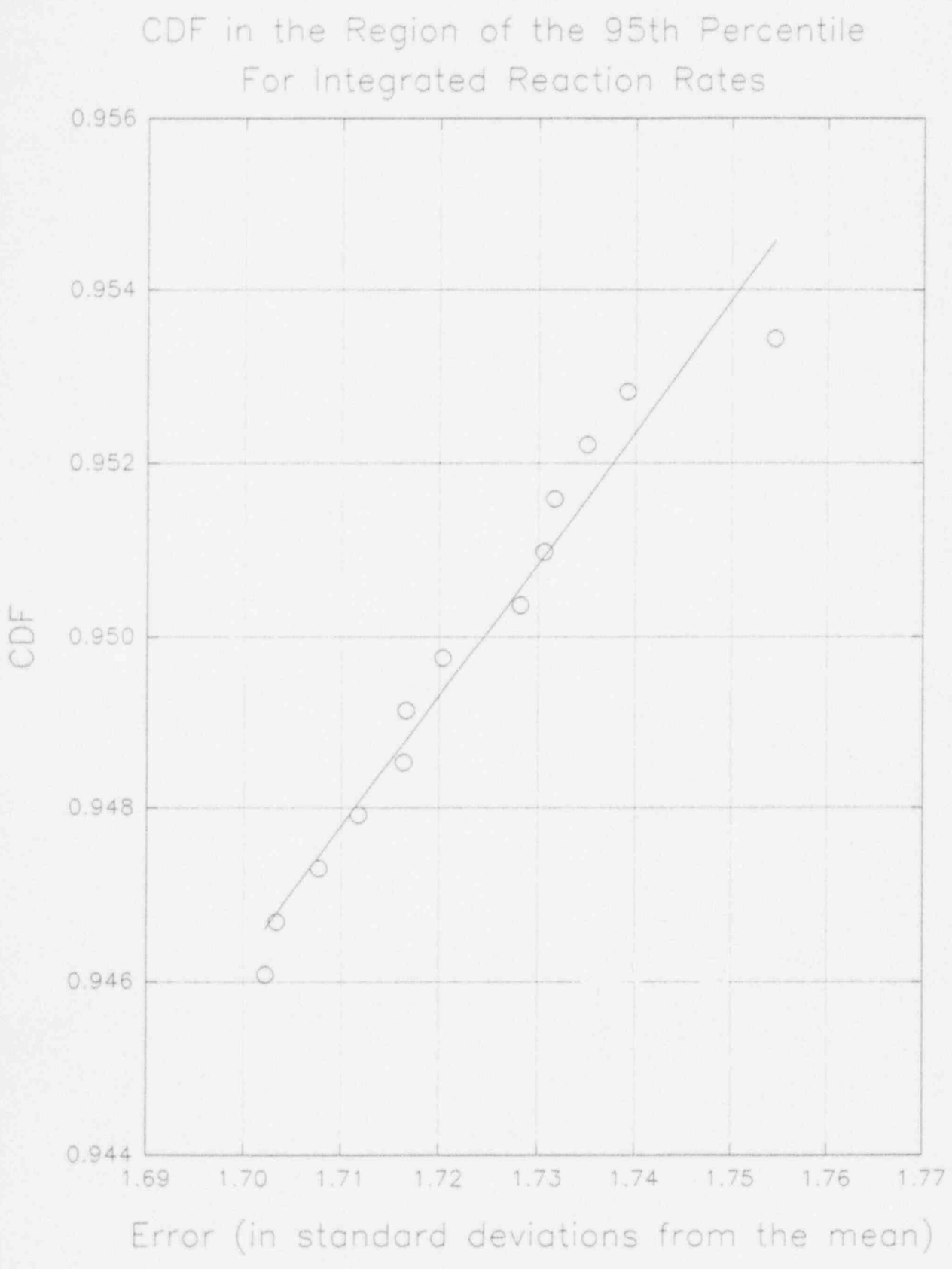
CDF in the Region of the 95th Percentile
For Integrated Reaction Rates
0.956
0.954
0.952
0.950
0.948
0.946
0.944
CDF
1.69
1.70
1.71
1.72
1.73
1.74
1.75
1.76
1.77
Error (in standard deviations from the mean)

Figure 3.6.22
Standard Deviation
vs Measured Instrument Response

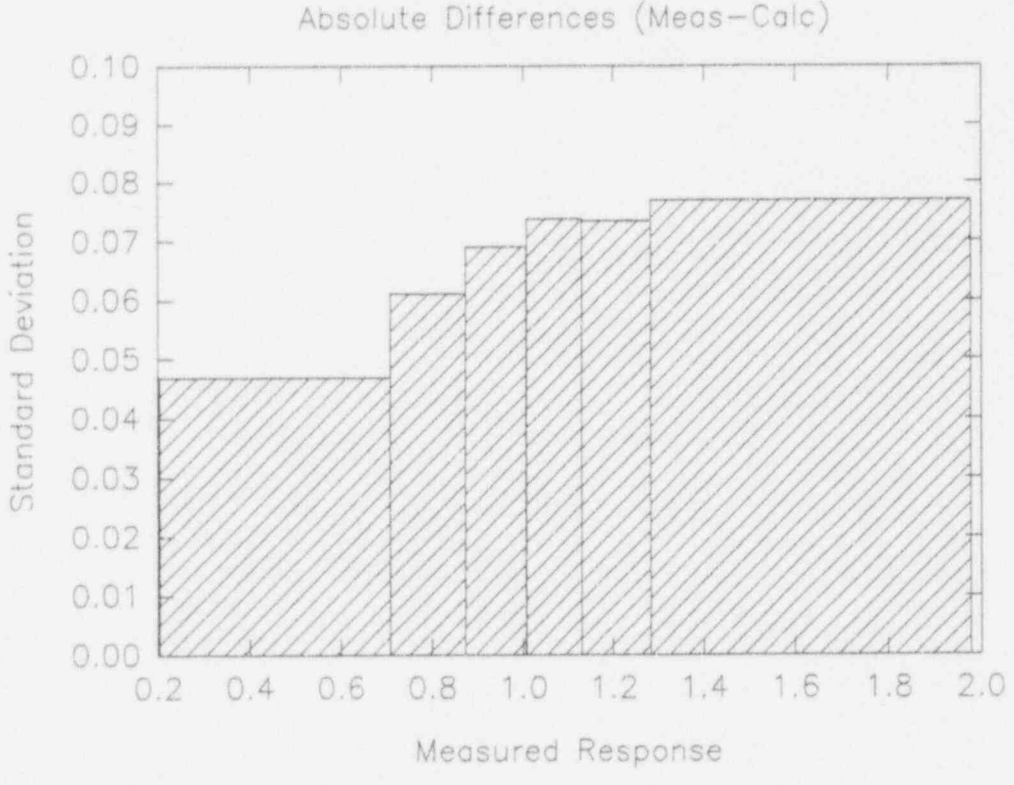

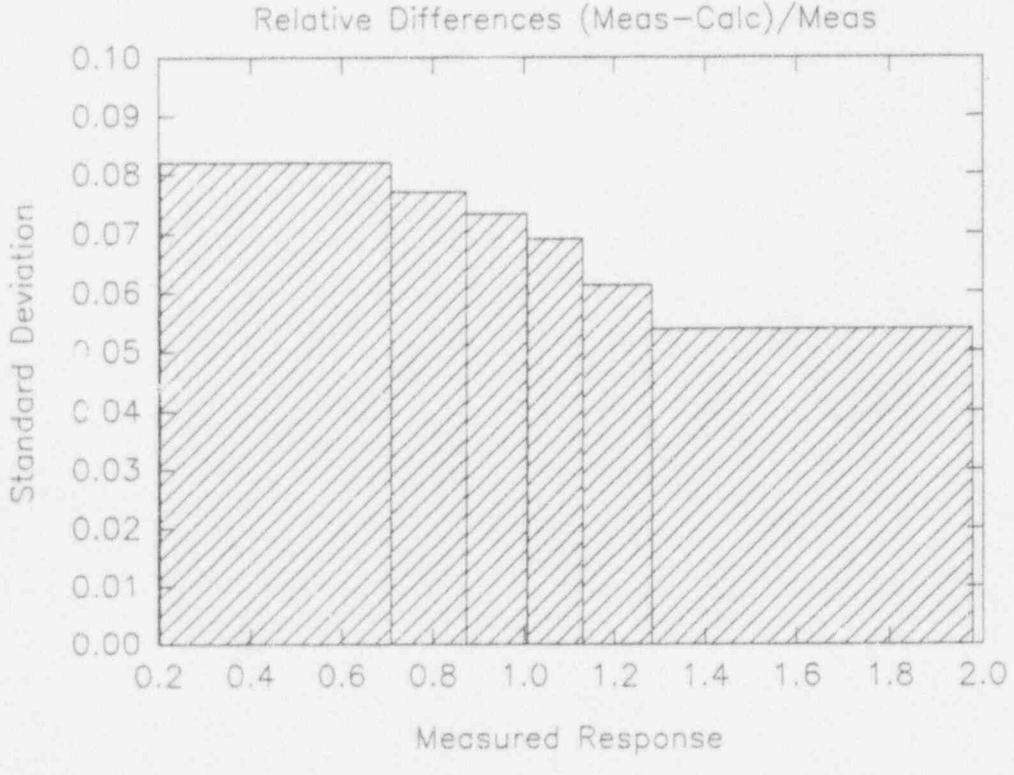

4.0 MODEL APPLICATIONS TO REACTOR OPERATIONS

This section describes the methods used in applying the reliability factors and biases to reactor operations. It is not the intent of this section to define the procedures used. However, some aspects of these procedures are presented in order to clarify the approach taken in applying the model reliability factors and biases.

The model will be applied to reactor operations in two primary modes, predictive and monitoring. Cold critical comparisons, including few rod and in-sequence criticals; and hot criticals at power are given below to verify this mode of application.

In the monitoring mode, process computer support and isotopic inventory calculations must be considered.

4.1 Predictive Applications

4.1.1 Cold Criticals

NSP has predicted few rod cold criticals around the high worth rod for each cycle of operation in order to verify the predicted model. The resultant cold critical k_{eff} for all few rod criticals calculated for cycles 11 through 15 is:

$$k_{eff} = 0.9929 \pm .0023$$

NSP has predicted in-sequence withdrawals to cold critical for each cycle of operation to verify the rod withdrawal pattern and to prevent the withdrawal of a high notch worth rod that could scram the reactor.

The resultant cold critical k_{eff} for all in-sequence criticals calculated for cycles 11 through 15 is:

$$k_{eff} = 0.9922 \pm .0028$$

The combined statistics of few rod and in-sequence criticals calculated for cycles 11 through 15 is:

$$k_{eff} = 0.9923 \pm .0027$$

Table 4.1.1 gives the detailed information for each critical.

Figure 4.1.1 gives the graphical representation of the criticals for each cycle.

4.1.2 Hot Full Power Criticals

NSP has predicted the hot at-power critical conditions throughout each cycle.

The resultant hot critical k_{eff} for all criticals calculated for cycles 11 through 15 is:

$$k_{eff} = 0.9979 \pm .0019$$

Table 3.6.1 gives the detailed information for each critical. Figure 4.1.2 gives the graphical representation of the criticals for each cycle. Circled points indicate coastdowns.

4.2 Monitoring Applications

4.2.1 Process Computer

The General Electric 3D-Monicore System recently installed at Monticello will be retained. NSP is currently evaluating several options for support of this system for cycles 18 and beyond. GE will supply support for cycle 17. The support options are as follows:

1. Continue to have GE supply all support.
2. NSP will support with system as installed.
3. NSP will support with system modified by replacing Panacea with an approved core model (i.e. SIMULATE-3 or NDH).

4.2.2 Isotopic Inventory

The isotopic inventory calculation will be performed by NSP if either option 2 or 3 is decided upon in Section 4.2.1. The calculation of the isotopic inventory for Monticello is based upon a two-dimensional, CASMO-3 calculation. This is the same model as is used to calculate the TIP trace design input. Therefore, the accuracy of the burnup distribution can be verified by the agreement of the measured and calculated reaction rates which is used to evaluate the measurement uncertainties, see Section 3.6 above. The accuracy of the isotopics versus local exposure is described in references 4 and 36 based on measurements at Yankee Rowe.

TABLE 4.1.1 Few Rod and In-sequence Cold Criticals

Cycle	Cycle Exposure (GWD/MTU)	Temperature (°F)	F = Few Rod S = Sequence	k_{eff}
11	0.000	85	F	0.9921
	0.000	106	F	0.9936
	0.000	106	S	0.9948
	0.000	113	S	0.9936
12	0.000	129	F	0.9964
	0.000	128	S	0.9928
	0.000	128	S	0.9938
	3.256	141	S	0.9903
	6.260	203	S	0.9896
13	0.000	91	F	0.9905
	0.000	91	F	0.9904
	0.000	91	S	0.9897
	0.000	91	S	0.9908
	8.853	201	S	0.9876
	9.764	164	S	0.9851
14	0.000	109	F	0.9907
	0.000	111	S	0.9913
	0.000	118	S	0.9936
	4.569	122	F	0.9924
	4.569	123	S	0.9919
	5.811	152	S	0.9895
	6.647	209	S	0.9905
	8.510	154	S	0.9923
	8.510	142	S	0.9920
15	0.000	108	F	0.9933
	0.000	108	F	0.9963
	0.000	113	S	0.9939
	0.000	107	S	0.9963
	0.093	200	S	0.9979
	0.093	147	S	0.9962
	1.616	182	S	0.9939
	4.151	137	S	0.9922
	6.202	129	S	0.9928

Statistics			
Type	N	Mean	σ
Few Rod	9	0.9929	0.0023
Sequence	24	0.9922	0.0028
Combined	33	0.9923	0.0027

Figure 4.1.1 Cold Criticals vs Core Average Exposure

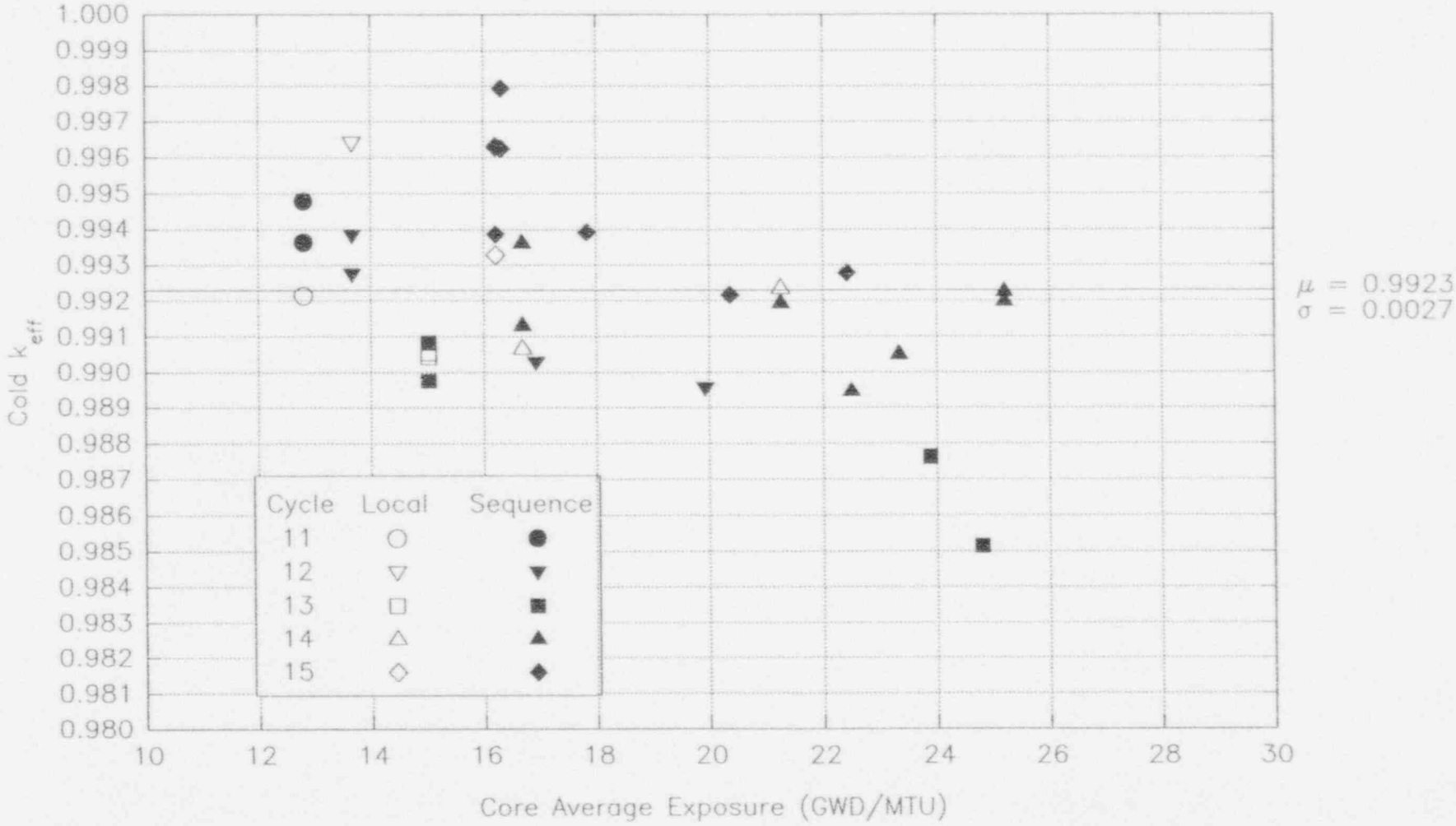

Figure 4.1.2 Hot Criticals

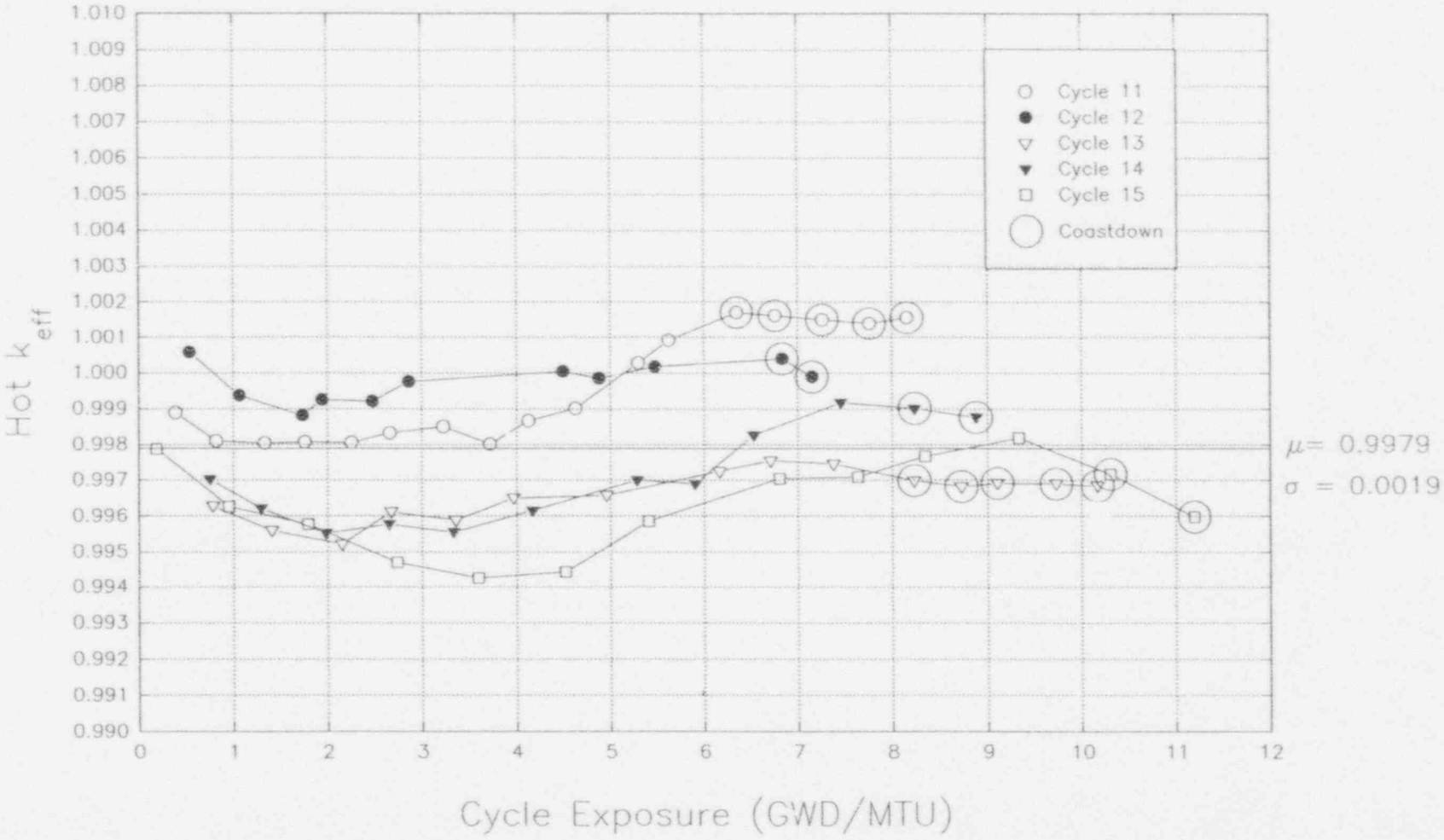

5.0 MODEL APPLICATIONS TO SAFETY EVALUATION CALCULATIONS

This section describes the methods used in applying the reliability factors and biases to the results of safety related physics calculations. It is not the intent of this section to define the procedures to be used in performing the physics calculations. However, some aspects of these procedures are presented in order to clarify the approach taken in applying the model reliability factors and biases.

In such applications, the question is generally: Will the reload core maintain a safe margin to established safety limits (i.e., peak linear heat generation rate, minimum CPR, shutdown margin, etc.) under normal and non-normal or accident conditions? The question is usually answered by performing cycle specific safety analyses for the limiting transients and accidents.

For each parameter of interest, RF_X and $Bias_X$ are given in Table 3.0.1. The application of the RF_X and $Bias_X$ for each parameter of interest is shown below.

5.1 Linear Heat Generation Rate (LHGR and APLHGR)

The Linear Heat Generation Rate (LHGR) and the Average Planar Linear Heat Generation Rate (APLHGR) are calculated directly in SIMULATE-3.

The model reliability factor and bias listed in Table 3.0.1 are then applied as follows:

$$LHGR = LHGR(model)\ (1 + Bias + RF_{TPF})$$

$$APLHGR = APLHGR(model)\ (1 + Bias + RF_{TPF})$$

where model signifies the best estimate value directly calculated with the 3D simulator.

5.2 Critical Power Ratio (CPR)

The Critical Power Ratio is defined as the ratio of the bundle power required to produce onset of transition boiling somewhere in the bundle (critical power) to the actual bundle power, i.e.:

$$CPR(I,J) = P_C(I,J) \ / \ P(I,J)$$

where:

$P_C(I,J)$ is the critical bundle power in assembly (I,J)
$P(I,J)$ is the actual bundle power in assembly (I,J)

The minimum critical power ratio, MCPR, is defined as the minimum value of CPR in the core, i.e.:

$$MCPR = (P_C(I,J) \ / \ (P(I,J))_{min}$$

The model reliability and bias listed in Table 3.0.1 are then applied as follows:

$$CPR = [P_C(I,J) \ / \ P(I,J)]\ (1 + Bias + RF_{RPF})]$$

5.3 Control Rod Worth

Rod worth are calculated using the three-dimensional nodal model. Worth are determined by varying the rod position while the independent core parameters such as core power, flow, and void distribution are held constant.

The model reliability factor and bias listed in Table 3.0.1 are then applied as follows:

$$\Delta K_{ROD} = \Delta K_{ROD}(MODEL)\ (1 + Bias)\ (1 \pm RF_{ROD})$$

The reliability factor is either added or subtracted, whichever is most conservative for each particular application.

5.4 Void Reactivity

The model reliability and biases listed in Table 3.0.1 are applied to $\Delta k/\Delta U$ as

$$\Delta k/\Delta U\ (1 + Bias)\ (1 \pm RF_{voids})$$

The reliability factor is either added or subtracted, whichever is most conservative, for each application.

5.5 Fuel Temperature (Doppler) Coefficient

The Doppler coefficient is a measure of the change in neutron multiplication associated with a change in fuel temperature. Reactivity is changed mainly due to Doppler broadening of the U-238 parasitic resonance absorption cross section due to increases in fuel temperature.

The model reliability factor and bias listed in Table 3.0.1 are then applied at each point as follows:

$$\Delta k/\Delta t_f^{1/2}\ (1 + Bias)\ (1 \pm RF_D)$$

Again, the reliability factor is either added or subtracted, whichever is most conservative for each particular application.

5.6 Delayed Neutrons

The delayed neutron constants; $ß_{eff,i}$ and λ_i, are assumed to be constant in time during a transient. The use of constant delayed neutron constants corresponding to the initial conditions is justified by the results in Reference 29 which show that $ß_{eff}$ does not change significantly during a transient until the scram is over. Adjoint flux weighting is used to obtain these constants.

The reliability factor listed in 3.0.1 is applied as shown:

$$ß_{eff,i}\ (model)\ (1 + Bias)\ (1 \pm RF_ß)$$

5.7 Prompt Neutron Lifetime

The prompt neutron lifetime Λ is assumed to be constant in time.

The reliability factor listed in Table 3.0.1 is applied as follows:

$$\Lambda(model)\ (1 + Bias)\ (1 \pm RF_\Lambda)$$

6.0 REFERENCES

1. NSP Topical "Qualification of Reactor Physics Methods for Application to PI Units", NSPNAD-8101P, Rev. 1, December, 1982.

2. NSP Topical "Qualification of Reactor Physics Methods for Application to Monticello", NSPNAD-8609, Rev. 1, April, 1992.

3. NSP Topical "Monticello Nuclear Generating Plant Safety Evaluation Methods," NSPNAD-8608, Rev. 1, August, 1988.

4. A. S. DiGiovine, K. B. Spinney, D. G. Napolitano, J. Pappas, "CASMO-3G Validation and Verification", YAEC-1653-A, Yankee Atomic Electric Company, 1990.

5. A. S. DiGiovine, J. P. Gorski, M. A. Tremblay, "SIMULATE-3 Validation and Verification", YAEC-1659-A, Yankee Atomic Electric Company, 1990.

6. B. Y. Hubbard, D. J. Morin, J. Pappas, R. C. Potter, "MICBURN-3/CASMO-3/TABLES-3/SIMULATE-3 Benchmarking of Cycles 9 Through 13," YAEC-1683-A, Yankee Atomic Electric Company, 1990.

7. M. Edenius, and B. H. Forssen, "CASMO-3 A Fuel Assembly Burnup Program User's Manual", Studsvik AB, NFA-89/3 Rev.2, March, 1992.

8. M. Edenius, H. Häggblom, and B. H. Forssen, "CASMO-3 A Fuel Assembly Burnup Program Methodology", Studsvik AB, NFA-89/2 Rev.1, January, 1991.

9. M. Edenius, A. Ahlin, and H. Häggblom, "CASMO-2 User's Manual, Studsvik AB, NR-81/3, 1981.

10. M. Edenius, and C. Grägg, "MICBURN-3 Microscopic Burnup in Burnable Absorber Rods User's Manual", Studsvik AB, NFA-89/12, November, 1989.

11. J. A. Umbarger, A. S. DiGiovine, K. S. Smith, and J. T. Cronin, "SIMULATE-3 Advanced Three-Dimensional Two-Group Reactor Analysis Code Users Manual", Studsvik of America, SOA-92/01 Rev.0, April, 1992.

12. K. S. Smith, J. T. Cronin, and J. A. Umbarger, "SIMULATE-3 Advanced Three-Dimensional Two-Group Reactor Analysis Code Methodology", Studsvik of America, SOA-92/02 Rev.0, April, 1992.

13. J. A. Umbarger, and K. S. Smith, "TABLES-3 Library Preparation Code for SIMULATE-3", Studsvik of America, SOA-92/03 Rev.0, April, 1992.

14. "S3POST SIMULATE-3 Summary File Postprocessor", Studsvik of America, SOA-91/04, 1991

15. I. B. Fiero, M. A. Krammen, H. R. Freeburn, et al, "ESCORE-The EPRI Steady-State Core Reload Evaluator Code: General Description", Electric Power Research Institute, EPRI NP-5100-L-A, April, 1991.

16. M. A. Krammen, H. R. Freeburn, et al, "ESCORE-The EPRI Steady-State Core Reload Evaluator Code Volume 1: Theory Manual", Electric Power Research Institute, EPRI NP-4492-CCMP Volume 1, August, 1986.

17. M. A. Krammen, R. B. Fancher, N. T. Yackle, et al, "ESCORE-The EPRI Steady-State Core Reload Evaluator Code Volume 2: User's Manual", Electric Power Research Institute, EPRI NP-4492-CCMP

Volume 2, August, 1986.

18. M. A. Krammen, R. B. Fancher, M. W. Kennard, et al, "ESCORE-The EPRI Steady-State Core Reload Evaluator Code Volume 3: Programmer's Manual", Electric Power Research Institute, EPRI NP-4492-CCMP Volume 3, August, 1986.

19. D. B. Jones, "ARMP-02 Documentation Part II, Chapter 7-MICBURN-E Computer Code Manual Volume 1: Theory and Numerics Manual", Electric Power Research Institute, EPRI NP-4574-CCM, Part II, Ch. 7 Volume 1, December, 1986.

20. D. B. Jones, "ARMP-02 Documentation Part II, Chapter 7-MICBURN-E Computer Code Manual Volume 2: User's Manual", Electric Power Research Institute, EPRI NP-4574-CCM, Part II, Ch. 7 Volume 2, December, 1986.

21. D. B. Jones, "ARMP-02 Documentation Part II, Chapter 7-MICBURN-E Computer Code Manual Volume 3: Programmers Manual", Electric Power Research Institute, EPRI NP-4574-CCM, Part II, Ch. 7 Volume 3, December, 1986.

22. M. Edenius, and H. Häggblom, "Benchmarking of CASMO Resonance Integrals for U-238 Against Hellstrand's Measurements", Studsvik of America, SOA-91/05, December, 1991.

23. M. A. Edenius, "Benchmarking of CASMO Resonance Integrals for U-238 Against Hellstrand's Measurements. Comparison between CASMO-3 Versions 4.4 and 4.7", Studsvik of America, SOA-93/04, March, 1993.

24. M. A. Edenius, "CASMO Doppler Coefficients versus MCNP-3A Monte Carlo Calculations", Studsvik of America, SOA-93/06, October, 1993.

25. M. Edenius, "Studies of the Reactivity Temperature Coefficient in Light Water Reactors," AE-RF-76-3160, AB Stomenergi, 1976.

26. M. Edenius, "Seminar on U-238 Resonance Capture," S. Pearlstein, Editor, page 87, BNL-NCS-50451, 1975.

27. M. Edenius, "Temperature Effects in Thermal Reactor Analysis," Internal Report presented to Oskarshamnuerkets Kraftgrupp AB(OKG), Stockholm, Sweden, employed by AB Stomenergi Studsvik, Sweden.

28. M. Edenius, and A. Ahlin, "CASMO-3: New Features, Benchmarking, and Advanced Applications," *Nuclear Science and Engineering*, 100, No. 3, p. 342, November, 1988.

29. J. M. Holzer, et.al. "A Code System to Produce Point Kinetics Parameters for LWR Calculations," *ANS Trans*, 39, 946-7, 1981.

30. M.G. Kendall, A. Stuart, "The Advanced Theory of Statistics," Vol. 1, 5th. ed., Hafner Publishing Co. N.Y., 1987.

31. D.B. Owen, "Factors for One-Sided Tolerance Limits and for Variables Sampling Plans" Sandia Corporation, March 1963.

32. K. S. Smith, "SIMULATE-3 Pin Power Reconstruction: Benchmarking Against B&W Critical Experiments," *Trans. Am. Nuc. Soc.*, 56, p. 531, San Diego, CA, June, 1988.

33. M. Edenius, "CASMO-3 Benchmarking," *Trans. Am. Nuc. Soc.*, 56, p. 536, San Diego, CA, June, 1988.

34. K. R. Rempe, K. S. Smith, and A. F. Henry, "SIMULATE-3 Pin Power

Reconstruction: Methodology and Benchmarking," *Nuclear Science and Engineering*, 103, No. 4, p. 334, December, 1989.

35. T. Uegata, E. Saji, and H. Tanaka, "Verification of the CASMO-3/SIMULATE-3 Pin Power Accuracy by Comparison with Operating Boiling Water Reactor Measurements," *Nuclear Science and Engineering*, 114, No. 1, p. 81, May, 1993.

36. P. J. Rashid, "CASMO-3 Benchmark Against Yankee Rowe Isotopics", Studsvik of America, SOA-86/05, September, 1986.

37. "Nuclear Design Methodology Using CASMO-3/SIMULATE-3P," Duke Power Company DPC-NE-1004A, November, 1992.

38. D. J. Edwards, L. E. Kostynak, F. A. Monger, R. M. Rubin, and C. E. Willingham, "Steady State Reactor Physics Methodology," Texas Utilities Electric Company, RXE-89-003-NP, July, 1989.

39. R. Y. Chang, C. W. Gabel, "PWR Reactor Physics Methodology Using CASMO-3/SIMULATE-3," Southern California Edison Company, SCE-9001-A, September, 1992.

40. M. Edenius and P. J. Rashid, "Benchmarking of the Gamma-TIP Calculation in CASMO Against the Hatch BWR," *Trans. Am. Nuc. Soc.*, 49, p. 431, Boston, MA, June, 1985.

41. K. S. Smith and K. R. Rempe, "Testing and Applications of the QPANDA Nodal Model," *Nuclear Science and Engineering*, 100, No. 3, p. 324, November, 1988.

42. A. S. DiGiovine and D. G. Napolitano, "SIMULATE-3 Pin Power Reconstruction and Comparison to Fine-Mesh PDQ," *Trans. Am. Nuc. Soc.*, 54, p. 361, Dallas, TX, June, 1987.

43. K. R. Rempe and K. S. Smith, "SIMULATE-3: Power Distributions and Detector Response Modeling," *Trans. Am. Nuc. Soc.*, 54, p. 355, Dallas, TX, June, 1987.

44. D. G. Napolitano, A. S. DiGiovine, K. R. Rempe, and K. S. Smith, "SIMULATE-3: Pin Power Reconstruction Applied to Seabrook Station," *Trans. Am. Nuc. Soc.*, 55, p. 590, Los Angeles, CA, November, 1987.

45. R. Hakanson and E. Kurcyusz-Ohlofsson, "Forsmark 1 Core Analysis with the Studsvik Code Package," *Proceedings of the 1988 International Reactor Physics Conference*, Jackson Hole, WY, September, 1988.

46. A. S. DiGiovine, J. P. Gorski, and M. A. Tremblay, "Verification of the SIMULATE-3 Pin Power Distribution Calculation.," *Nuclear Science and Engineering*, 103, No. 4, p. 324, December, 1989.

47. E. Kurcyusz-Ohlofsson, "Analysis of Advanced PWR Cores with CASMO-3/SIMULATE-3," PHYSOR 90, Vol.2, p. XIV-1, Marseille, France, April, 1990.

48. K. S. Smith and K. R. Rempe, "Mixed-Oxide and BWR Pin Power Reconstruction," PHYSOR 90, Vol.2, p. VII-11, Marseille, France, April, 1990.

49. H. Grubel, R. Rippler, G. Skoff, B. Wikes, and G. Wupperfeld, "Umstellung der nuklearen Kernausleng für das KKW Mülheim-Kärlich (KMK) auf das Studsvik-Programmsystem CASMO/SIMULATE," *Tagungsbericht Proceedings*, Jahrestagung Kerntechnik '91, p. 3, Bonn, Germany, May, 1991.

50. Y. Wang, J. Yang, Y. Yeh, and S. Yaur, "Neutronic Model Verification for Maanshan Power Plant with Advanced In-core Fuel Management Package," *Proceedings of the 1992 Topical Meeting on Advances in Reactor Physics*, p. 1-13, Charleston, SC, March, 1992.

51. A. Jonsson, D. R. Harris, R. Y. Chang, O. J. Thomsen, "Analysis of Critical Experiments with Erbia-Urania Fuel," *Trans. Am. Nuc. Soc.*, 65, p. 415, Boston, MA, June, 1992.

APPENDIX A Statistical Methods for the Determination and Application of Uncertainties

The purpose of using statistical methods is to determine the value X_C (calculated) such that there is a 95% probability at the 95% confidence level that X_C will be conservative with respect to X_T (true value) when applying the calculational methods to safety related reactor analyses.

The first step is to determine whether or not a distribution is normal. If it is, the methods described in Section A.1 are used. If the distribution cannot be treated as normal, but the distributions are known, then the methods described in Section A.2 are used.

If neither of the above methods apply, then the parameter in question is conservatively bounded.

A.1 Application of Normal Distribution Statistics

Separation of Measurement and Calculational Uncertainties

Comparison of measured and calculated reactor parameters includes the effects of both the measurement and calculational uncertainties. Methods used in this report to isolate the calculational uncertainties are described below in terms of the following definitions:

X_t = true reactor parameter

X_m = measured reactor parameter

X_c = calculated reactor parameter

$e_m = (X_m - X_t) / X_t$ = measurement error

$e_c = (X_c - X_t) / X_t$ = calculation error

$e_{mc} = (X_m - X_c) / X_m$ = observed differences

$$\mu = \frac{\sum_{i=1}^{n} e_i}{n}$$

$$\sigma = \left(\sum_{i=1}^{n} (e_i - \mu_i)^2\right) / (N-1))^{1/2} = \textit{standard deviation}$$

If e_m and e_c are independent, then the follcwing relationships exist. (Note that these relationships apply for non-normal distributions as well).

$$\sigma_c^2 = \sigma_{mc}^2 - \sigma_m^2$$

$$\mu_c = \mu_c - \mu_{mc}$$

Once the σ_c and μ_c have been calculated from historical data, they could be used to apply conservatism to future calculations of reactor parameters, X_c, as follows:

$$X_c \rightarrow X_c (1 + \mu_c) (1 \pm K_c \sigma_c)$$

The factor K_c is defined as described in Table A.1.14 to provide a 95% probability at the 95% confidence level that X_c is conservative with respect to the true value, X_t.

Reliability Factors

It is the objective to define reliability factors which are to be used to increase/decrease calculated results to the point where there is a 95% probability at the 95% confidence level that they are conservative with respect to actual reactor parameters.

For any given application, there is concern only with one side of the component; that is, if the calculated value is too large or too small.

Therefore, one-sided tolerance limits based on normal distributions may be used to find a K_c which will give a 95% probability at the 95% confidence level to the reliability factor defined by:

$$RF = K_c \sigma_c$$

Numerical values of K_c for various sample sizes used to calculate σ_c are provided on Table A.1.

TABLE A.1 Single-Sided Tolerance Factors (Reference 31)

n	K_c
2	26.26
3	7.66
4	5.15
5	4.20
6	3.71
7	3.40
8	3.19
9	3.03
10	2.91
11	2.82
12	2.74
15	2.57
20	2.40
25	2.29
30	2.22
40	2.13
60	2.02
100	1.93
200	1.84
500	1.76
∞	1.645

n = Number of data points used for σ

A.2 Application of Non-Normal Distribution Statistics

If a distribution is determined to be other than normal, the requirement is that there is a 95% confidence level that X_c will be conservative with respect to the true value X_m. (In the following, the notation used is consistent with that defined in Section A.1). It is thus required that a 95% upper confidence limit be determined for the 95th percentile of the distribution of errors.

In the calculation, a set of error observations (e_i) are determined. The mean (μ_{mc}) and the standard deviation (σ_{mc}) are calculated using the following formulation:

$$\mu_{mc} = \frac{\sum_{i=1}^{n} e_i}{n}$$

$$\sigma_{mc} = \left(\left(\sum_{i=1}^{n} (e_i - \mu_{mc})^2\right) / (n-1)\right)^{1/2}$$

Note that the e_i above are determined from the following:

$$e_i = e_{mc} = (X_m - X_c)/X_m = \textit{observed differences}$$

Generally, the e_{mc} are taken from several cycles of operation; thus, they represent the true distribution. The e_i are then transformed to standard measure by the following formula:

$$Z_i = \frac{e_i - \mu_{mc}}{\sigma_{mc}}$$

and the resulting variates (Z) are sorted into ascending order and the kth (such that $k \geq .95n$) variate is chosen as an estimate of the 95th percentile of the distribution (See reference 30, page 50-51). This gives a 95th percentile of Z to be Q_{95}. This implies that 95% of the errors are likely to be less than Q_{95}.

It remains to calculate a 95% confidence interval on Q_{95}. (The formula for this calculation is taken from reference 13 page 236-243 (See references section 6.0).

$$Var\ Q_{95} = \frac{q(1-q)}{n\, f_1^2}$$

where: q = the quantile (.95)
n = number of independent observations in the sample
f_1 = ordinate of the density function of the distribution of observed differences at abscissa q

It is necessary to determine if the observations are independent. If they are not independent, it is necessary to reduce the sample size to account for the dependence in the determination of the 95% confidence level.

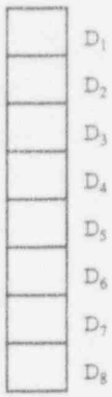

Figure A.2.1. Differences for Nearby Positions

To set notation, let δ_{95} be the population 95th percentile for the observed differences, that is $P[D_i \leq \delta_{.95}] = .95$. We wish to determine a 95% upper confidence limit for δ_{95} when some of the differences are dependent. For differences observed at adjacent positions, the appropriate measure of association for our analysis can be shown to be

$$C(1) = P[D_1 \leq \delta_{.95} \text{ and } D_2 \leq \delta_{.95}] - (.95)^2$$

We also consider the association of differences observed at locations two apart

$$C(2) = P[D_1 \leq \delta_{.95} \text{ and } D_3 \leq \delta_{.95}] - (.95)^2$$

and, more generally,

$$C(k) = P[D_1 \leq \delta_{.95} \text{ and } D_{1+k} \leq \delta_{.95}] - (.95)^2$$

for k = 1,2,3,4,5,6,7 locations apart. In this example, there are 8 differences D_i, 7 adjacent pairs (D_i, D_{i+1}), 6 pairs with indices two apart (D_i, D_{i+2}) ..., 1 pair D_1D_8.

Let $d_{(s)}$ be the sample 95th percentile with s selected to be the smallest integer not less than .95n. The large sample distribution of $d_{(s)}$ depends on that of

T(x) = number of differences, D_i, that are less than or equal x.

Even with dependence among the D_i,

$$\frac{T(x) - nF(x)}{s.d.[T(x)]} = \frac{\frac{1}{\sqrt{n}}(T(x) - nF(x))}{\frac{1}{\sqrt{n}} s.d.[T(x)]}$$

will be approximately standard normal. Here $F(x) = P[D_i \leq x]$ and $f(x)$ is the probability density function for the observed differences.

It follows that

$$P[\sqrt{n}(d_{(s)} - \delta_{.95}) \leq z] = 1 - P[T(\delta_{.95} + n^{-1/2}z) \leq s-1]$$

$$\approx 1 - \Phi\left[\frac{-f(\delta_{.95})\,z}{\frac{1}{\sqrt{n}}\; s.d[T(\delta_{.95})]}\right]$$

where

$$[\frac{1}{\sqrt{n}}\; s.d.[T(\delta_{.95})]]^2 = \frac{1}{n}[n(.95)(.05) + 2\,\frac{7}{8}nC(1) + 2\,\frac{6}{8}nC(2) + \ldots\, \frac{2}{8}nC(7)]$$

$$= (.95)(.05) + \frac{14}{8}C(1) + \frac{12}{8}C(2) + \frac{10}{8}C(3) + \ldots\, \frac{2}{8}C(7)$$

Under independence $0 = C(1) = C(2) = \ldots = C(7)$ and this expression reduces to its customary value $(.95)(.05)$. If the differences are dependent, the variance of $d_{(s)}$ is

$$\frac{(.95)(.05)}{nf^2(\delta_{.95})}\left[1 + \sum_{k=1}^{7}\; \frac{2(8-k)\,C(k)}{8(.95)(.05)}\right]$$

In order to apply this result, we estimate $C(1)$ by

$$C(1) = \frac{number\ of\ adjacent\ pairs\ (D_i, D_{i+1})\ where\ both \leq d_{(s)}}{Total\ number\ of\ adjacent\ pairs} - (.95)^2$$

The estimate of $C(2)$ is

$$C(2) = \frac{number\ of\ pairs\ (D_i, D_{i+2})\ where\ both \leq d_{(s)}}{Total\ number\ of\ pairs\ (D_i, D_{i+2})} - (.95)^2$$

and

$$C(k) = \frac{number\ of\ pairs\ (D_i, D_{i+k})\ where\ both \leq d_{(s)}}{Total\ number\ of\ pairs\ (D_i, D_{i+k})} - (.95)^2$$

for $k = 3,4,5,6,7$. The value of $f^2(\delta_{.95})$ can be estimated as previously suggested. Then, the large sample upper 95% confidence limit for $\delta_{.95}$, adjusted for dependence among differences by location is given by

$$d_{(s)} + \frac{1.645}{\sqrt{n}}\left[\frac{(.95)(.05)}{f^2(\delta_{.95})}\left(1 + \sum_{k=1}^{7}\; \frac{2(8-k)\,C(k)}{8(.95)(.05)}\right)\right]^{1/2}$$

One interpretation of this confidence limit, or the variance expression, is that the total sample size n is effectively reduced by the dependence. We estimate the effective sample size to be

$$\frac{n}{1 + \sum_{k=1}^{7} \frac{2(8-k)C(k)}{8(.95)(.05)}}$$

If only two terms are used, the effective sample size is estimated to be

$$n\left[\frac{(.95)(.05)}{(.95)(.05) + \frac{14}{8}C(1) + \frac{12}{8}C(2)}\right]$$

It is necessary to obtain an estimate of f_1 (.95) on a short interval of the cumulative distribution function of Z in the region of the 95th percentile. The slope of the cumulative distribution function is an estimate of the ordinate of the density function since the density function is simply the derivative of the cumulative distribution function. Thus

$$\sigma^2_{Q_{95}} = Var\ Q_{95}$$

This value then allows an estimate of the 95% confidence limit on Q_{95}. Even though nothing is known about the distribution of Q_{95}, the distribution can be shown to be normal using the following derivation.

$$P[D_1 \le \delta_{.95}\ and\ D_2 \le \delta_{.95}]$$

where δ_{95} is the 95th percentile of the distribution of differences. If the differences D_1 and D_2 are independent

$$P[D_1 \le \delta_{.95}\ and\ D_2 \le \delta_{.95}] = P[D_1 \le \delta_{.95}]\ P[D_2 \le \delta_{.95}]$$
$$= (.95)(.95) = (.95)^2$$

The difference

$$P[D_1 \le \delta_{.95}\ and\ D_2 \le \delta_{.95}] - (.95)^2$$

is a measure of association (dependence) from position to adjacent position. Note that if

$$I(D_1 \le \delta_{.95}) = \begin{cases} 1\ if\ D_1 \le \delta_{.95} \\ 0\ if\ D_1 > \delta_{.95} \end{cases}$$
$$I(D_2 \le \delta_{.95}) = \begin{cases} 1\ if\ D_2 \le \delta_{.95} \\ 0\ if\ D_2 > \delta_{.95} \end{cases}$$

then the covariance is

$$C(1) = Cov(I(D_1 \le \delta_{.95}), I(D_2 \le \delta_{.95})) = P[D_1 \le \delta_{.95}\ and\ D_2 \le \delta_{.95}] - (.95)^2$$

We <u>assume</u> the same covariance for

$I(D_2 \le \delta_{.95})$ and $I(D_3 \le \delta_{.95})$ ... $I(D_7 \le \delta_{.95})$ and $I(D_8 \le \delta_{.95})$.

There are about n 7/8 such pairs among the whole set of n observed

differences.

Let $d_{(s)}$ be the sample 95th percentile where s is the smallest integer not less than n(.95). When n is large

$$C(1) = \frac{number\ of\ pairs\ (D_i, D_{i+1})\ where\ both \le d_{(s)}}{Total\ number\ of\ pairs\ (D_i, D_{i+1})} - (.95)^2$$

is a good estimate of C(1). Similarly, for the approximately 6n/8 pairs (D_i, D_{i+2})

$$C(2) = Cov[I(D_1 \le \delta_{.95}), I(D_3 \le \delta_{.95})]$$

is estimated by

$$C(2) = \frac{number\ of\ pairs\ (D_i, D_{i+2})\ where\ both \le d_{(s)}}{Total\ number\ of\ pairs\ (D_i, D_{i+2})} - (.95)^2$$

and

$$C(k) = \frac{number\ of\ pairs\ (D_i, D_{i+k})\ where\ both \le d_{(s)}}{Total\ number\ of\ pairs\ (D_i, D_{i+k})} - (.95)^2$$

Let us now see how to modify the proof that $d_{(s)}$ is asymptotically normal in order to account for the dependence among adjacent differences. It is still true that

(A1)
$$\begin{aligned} P[d_{(s)} \le x] &= 1 - P[d_{(s)} > x] = 1 - P[s-1\ or\ fewer\ D_i \le x] \\ &= 1 - P[T(x) < s] \end{aligned}$$

where $T(x) = \sum_{i=1}^{n} I(D_i \le x)$ = # differences $D_i \le x$. Moreover, T(x) - nF(x) has mean 0 and, for large samples, is approximately normal under a wide range of dependence structures. Consequently, the

sums $\sum_{i=1}^{8} I(D_i \le x)$ are independent of one another and each has the same distribution. Since T(x) is just the sum of these group sums, the central limit theorem gives

$$\frac{T(x) - nF(x)}{s.d.[T(x)]} \quad \text{is approximately standard normal.}$$

Consequently, from (A1) and the normal approximation

(A2)
$$\begin{aligned} P[\sqrt{n}(d_{(s)} - \delta_{.95}) \le Z] &= P[d_{(s)} \le \delta_{.95} + n^{-1/2}Z] \\ &= 1 - P[T(\delta_{.95} + n^{-1/2}Z) < s] \\ &= 1 - \Phi\left[\frac{s - nF(\delta_{.95} + n^{-1/2}Z)}{s.d.[T(\delta_{.95} + n^{-1/2}Z)]}\right] \end{aligned}$$

Now, note that

$$\frac{1}{\sqrt{n}}(s-nF(\delta_{.95}+n^{-\frac{1}{2}}z)) = \frac{1}{\sqrt{n}}(s-nF(\delta_{.95}) - nf(\delta_{.95})n^{-\frac{1}{2}}z+0(1))$$
$$= \frac{1}{\sqrt{n}}(s-n(.95) - n^{\frac{1}{2}}zf(\delta_{.95})) + 0(1)$$
$$= -zF(\delta_{.95}) + 0(1)$$

Furthermore,

$$\frac{1}{n}Var[T(\delta_{.95}+n^{-\frac{1}{2}}z)] = Var[I(D_1 \le \delta_{.95}+zn^{-\frac{1}{2}})]$$
$$+\sum_{k=1}^{7}\frac{2(8-k)}{8}Cov[I(D_1 \le \delta_{.95}+n^{-\frac{1}{2}}z), I(D_{1+k} \le \delta_{.95}n^{-\frac{1}{2}}z)]$$

which converges to

$$F(\delta_{.95})-F^2(\delta_{.95}) + \sum_{k=1}^{7}\frac{2(8-k)}{8}\{P[D_1 \le \delta_{.95}, D_{1+k} \le \delta_{.95}] - (.95)^2\}$$
$$= (.95)(.05) + \sum_{k=1}^{7}\frac{2(8-k)}{8}C(k) = \lim\frac{1}{n}Var[T(\delta_{.95})]$$

Therefore, by (A2),

$$P[\sqrt{n}(d_{(s)} - \delta_{.95}) \le z] \sim 1-\Phi\left[\frac{-zf(\delta_{.95})}{\frac{1}{\sqrt{n}}s.d.[T(\delta_{.95})]}\right]$$

or $\sqrt{n}(d(s) - \delta_{95})$ is approximately normal with mean 0 and variance

$$\frac{1}{n}\left[\frac{(.95)(.05)+\sum_{k=1}^{7}2(8-k)C(k)/8}{f^2(\delta_{.95})}\right]$$

As was indicated above, the C(k) may be estimated by C(k) and the large sample normality will still hold. Therefore using Table A.1 to obtain K_c:

$$\lambda_{Q_{95}} = K_c(Var\ Q_{95})^{\frac{1}{2}}$$

Thus it is 95% certain that Q_{95} lies in the interval

$$Q_{95} \le Q_{95} + \lambda\sigma Q_{95}$$

therefore it is safe to say that we are 95% confident that the 95th percentile of the differences is:

$$\mu_{mc} + \sigma_{mc.95} \le \mu_{mc} + (Q_{95} + \lambda\sigma Q_{95})\sigma_{mc}$$

APPENDIX B Computer Code Summary Description

COMPUTER CODE	DESCRIPTION
CASMO-3	CASMO-3 is a multigroup two-dimensional transport theory code for depletion and branch calculations for a single assembly. It calculates the cross sections, nuclide concentrations, pin power distributions, and other nuclear data used to calculate input to the SIMULATE-3 program. Some of the characteristics of CASMO-3 are: 1. 40 energy group cross section library. 2. 7 energy groups are used during the two-dimensional transport calculations. 3. Gadolinium effective cross sections are generated by the MICBURN-3 program. 4. The predictor-corrector approach is used for depletion. 5. Effective resonance cross sections are calculated individually for each pin.
ESCORE	ESCORE is a steady-state fuel performance code capable of modeling the thermal and mechanical response of LWR fuel and used to provide fuel temperature inputs.
MICBURN-3	MICBURN-3 calculates the burnup of a fuel pin containing gadolinium and generates 40 group effective cross sections as a function of number density for gadolinium to be input to CASMO-3.
SIMULATE-3	A two-group 3D nodal program based on the QPANDA neutronics model. Some of the features of SIMULATE-3 are: 1. Explicit reflector cross model. 2. Pin power reconstruction. 3. Fourth order expansion of intranodal flux distribution. 4. No input normalization from higher order calculations or benchmark results.
SPM	Receives input from S3POST of the predicted, measured, and difference of the TIP reaction rates and calculates the biases and reliability factors.
S3POST	Reads output SIMULATE-3 and generates summaries and comparisons to measured incore TIP response. Modified by NSP to generate a file containing measured and predicted incore TIP response for input to the SPM program.
TABLES-3	Reads CASMO-3 output files and generates the input tables and curve fits for each fuel type for the SIMULATE-3 computer program.